CHALMERS

Model Based Haptic Feedback Design for Articulated Vehicle

Master's Thesis in Systems, Control & Mechatronics

ROBERT FREIHOLTZ
MÅNS PIHLSGÅRD

Department of Signals & Systems
Chalmers University of Technology
Gothenburg, Sweden 2015
Master's Thesis 2015:1

Abstract

This thesis investigates and develops a haptic feedback solution for a wheel loader by designing and constructing a prototype joystick. The main reason for haptic feedback is to improve the manoeuvrability of Steer-By-Wire systems. The design includes modelling, prototyping and control over the joystick and modelling and control over a vehicle model. The final result was a joystick in one dimension that controlled a vehicle model run on a Arduino DUE, the vehicle was then presented on a computer screen for the user.

The haptic feedback was broken down into several tasks to help the design of the controllers, tracking of vehicle angle, vehicle velocity based friction, a centring force and a simulated mechanical stop. The latter was to be able to use the joystick in different vehicles which potentially could have different maximum steering angle. The conclusion was a PD controller for the angular tracking, since that would allow steering and still restrict fast movement and deviation from the vehicle angle. The friction and the centring controllers were P controllers that used angular velocity and angle to control, the reference was to keep each state to zero. The feel of the haptic feedback was smooth and felt natural. For the mechanical stop an event based controller was used. The controller is an open loop controller that used a predefined impact pattern which is dependent on the speed of the joystick at impact, this provided a sharp stop without significant overshoot. The open loop allows for a control signal with higher frequency components than a closed loop system with the corresponding sampling time. Different versions of P, PI or PD controllers were tested for the mechanical stop but deemed to sluggish or aggressive to be of use.

The conclusion is that in order to establish a realistic mechanical stop an open loop response feels much more realistic than a closed loop controller, this is due to the high frequency components that makes up the impact of a mechanical stop. To make a realistic closed loop response an extremely high sampling rate is needed. For tracking purposes a PD controller provided a realistic behaviour as the controller would act passively and only restrict fast movement in comparison to an integrating controller which would be aggressive and feel active.

KEYWORDS: Haptic Feedback, Force Feedback, Steer-By-Wire, Event Based Control, Simulated Mechanical Stop, Articulated Vehicle, Dynamic Modelling, Arduino, PID, LQR, Joystick

Preface

This Master's Thesis was carried out at CPAC Systems AB located in Gothenburg, Sweden, during the fall semester of 2014. CPAC Systems AB is a part of the Volvo Group.

Acknowledgements

The authors would like to give a special thank to their supervisor at Chalmers University of Technology, Balázs Adam Kulcsár, for his continuous support throughout the project, Reine Nohlborg from the Prototype Lab at Chalmers University of Technology for his help creating the custom parts needed for assembly. Special thanks to CPAC Systems AB for giving the authors the opportunity to work with this project. The authors would also like to thank their friend Samir Lövgren for supplying the authors with replacement parts for the fried circuits produced during this thesis.

Robert Freiholtz and Måns Pihlsgård, Gothenburg 2015-03-20

Contents

Nomenclature

PID	Proportional-Integral-Derivative controller.
γ	Steering angle of the vehicle.
ϕ	Angle of the joystick.
θ	Angle between the vehicle and a global x axis.
θ_1	Angle between the front of the vehicle and a global x axis.
θ_2	Angle between the back of the vehicle and a global x axis.
l_1	Length from the front wheel axle of the vehicle to the articulated joint.
l_2	Length from the back wheel axle of the vehicle to the articulated joint.
l_{cg1}	Length from centre of gravity for the front part of the vehicle to the articulated joint.
l_{w1}	Length from the centre of the front wheel axle of the vehicle to the wheels.
l_{cg2}	Length from the centre of gravity for the back part of the vehicle to the articulated joint.
l_{w2}	Length from the centre of the back wheel axle of the vehicle to the wheels.
$\dot{\gamma}$	Angular velocity for the steering angle.
LQR	Linear-Quadratic Regulator.
$\ddot{\gamma}$	Angular acceleration for the steering angle.
$\dot{\phi}$	Angular velocity for the joystick.
$\ddot{\phi}$	Angular acceleration for the joystick.
m_1	Mass of the front part of the vehicle.

m_2	Mass of the back part of the vehicle.
$\dot{x_1}$	Longitudinal velocity of the front part of the vehicle.
$\dot{x_2}$	Longitudinal velocity of the back part of the vehicle.
$\dot{y_1}$	Lateral velocity of the front part of the vehicle.
$\dot{y_2}$	Lateral velocity of the back part of the vehicle.
$\ddot{x_1}$	Longitudinal acceleration of the front part of the vehicle.
SISO	Single-Input Single-Output.
$\ddot{x_2}$	Longitudinal acceleration of the back part of the vehicle.
$\ddot{y_1}$	Lateral acceleration of the front part of the vehicle.
$\ddot{y_2}$	Lateral acceleration of the back part of the vehicle.
L	The total energy of the system.
T	The total kinetic energy of the system.
V	The total potential energy energy of the system.
Q_x	Generalised forces in the along the x axis.
Q_y	Generalised forces in the along the y axis.
Q_θ	Generalised torque in θ.
Q_γ	Generalised torque in γ.
MISO	Multiple-Input Single-Output.
DC	Direct current.
GUI	Graphical user interface.
USB	Universal Serial Bus.
Simscape	Simulink toolbox, for modeling and simulating physical systems spanning mechanical, electrical, hydraulic, and other physical domains. Read more in [1].
Arduino	Arduino is an open-source electronics platform based on hardware and software. Read more in [2].
LHD	Load Haul Dump.
FBW	Fly-By-Wire.

Q_{wx}	Weight matrix in LQR respect to states.
CPU	Central Processing Unit.
Q_{wu}	Weight matrix in LQR respect to control signal.
AD	Analog-to-Digital.
IO	Input/Output.
PWM	Pulse-Width Modulation.
SBW	Steer-By-Wire.

1

Introduction

Haptic feedback, the word haptic relates to the Greek language and means to touch, come in contact with. In vehicles the major haptic feedback device is the steering device. This is usually connected through rods and gears to the wheels and allows the driver to both steer the vehicle and to feel the resistance of the road etcetera, the driver will also get a visual feedback. The throttle is another device with some sense of haptic, though not as straight forward, when the pedal is pressed the driver experience a pushing force due to acceleration and he will hear the sound of the engine. All these senses will help the operator to control the vehicle. Some of the senses could be removed without altering the manoeuvrability of the vehicle while others, for example the vision, would greatly affect the control of the vehicle. Another example where the haptic feedback can improve the control is the following, if a fork lift placing a pallet gets stuck or hits an object that is hidden from the drivers view he might push even harder on the controls and damage the loaded package. If the driver could sense the resisting force acting on the pallet the situation could possibly be avoided [3].

Modern development in computers have made it possible for Steer-By-Wire (SBW) to be implemented in vehicles, both construction equipment and commercial vehicles. One of the main reasons for SBW is the modularity of such a system, components can be moved to improve ergonomics, weight balance or be rearranged to fit in a small contained area. Weight reduction is also an advantage of changing to SBW [4]. The SBW technique opens up for many interesting choices of steering, from the conventional steering wheel and joystick to differential steering dependent on the velocity or other parameters, such as forces, moments etcetera. The main disadvantage of SBW is that it disconnects the direct contact between the operator and the surrounding environment, in essence removing some of the drivers senses of the vehicle. While this is sometimes sought to minimise stress or shaking it can lead to decreased accuracy in controlling the vehicle. The operator might overcompensate the controls if unable to properly assess the situation. In

order to heighten the drivers awareness some sensing feature must be added. This sense can be consisting of different types of senses, audio, visual and tactile feedback. Most cases involve a visual sense and sometimes sensing through sound. These two combined work very well for most applications. Overcompensating steering can potentially be dangerous, especially when transporting dangerous goods or heavy machinery. This is where the haptic feedback can improve the safety and manoeuvrability of the vehicle. It would also be possible to give preemptive feedback based on proximity to an object. This gives the operator a direct sense of the control task and improves the possible accuracy [5]. In the later years haptic feedback systems have entered the construction equipment branch, mainly in trucks and heavy machines [6].

1.1 Problem Specification

A vehicle that sometimes is equipped with both a steering wheel and a joystick is a wheel loader, which is a articulated vehicle, seen in figure 4.1. Different variations of SBW devices both with and without haptic feedback for steering wheels exists for this type of vehicle. This thesis will evaluate a haptic feedback solution using a joystick as steering device, as well as the manner of steering of the vehicle, if the vehicle should be steered by turning speed or by angle tracking. The thesis will focus on the following topics:

- Joystick design
- Feedback controller
- Modelling of vehicle
- Modelling of joystick
- Simulations with attached joystick

The joystick should be designed using an approach which considers both haptic feedback and functionality. Functionality demands on the joystick are that it should be able to provide sufficient torque in order to simulate a mechanical stop and that the size and the power consumption should not be unreasonably high considering that the application should be possible to place inside the machine.

The haptic feedback in this thesis should mimic a physical link between the joystick and the vehicle. Since haptic feedback is a subjective problem, the control focuses more on the actual feeling of controlling the joystick than it focuses on the accurate controller tracking. Therefore the sought haptic feedback will be broken down into four sub tasks:

1 - Tracking

The steering angle of a steering device physically connected to the vehicle would not deviate from the vehicle at any great extent. So the angle of the joystick should track the angle of the vehicle, while still allow steering.

2 - Mechanical Stop

Since the maximum steering of a vehicle differs for different models, the joystick can not have a mechanical stop for each and still be considered modular. To make the joystick independent of the type of vehicle, a mechanical stop should be simulated for the joystick.

3 - Centring

The joystick will have a centring behaviour when, straightening the vehicle while moving forward. This behaviour is known to people familiar with driving a car. This was selected as a task even though is contradictory to the real behaviour of an articulated vehicle.

4 - Friction

Steering a vehicle at different velocities is associated with a different resisting forces. This velocity dependent restricting forces could be viewed as frictions. Therefore a velocity depended friction is also a sought out feeling in this device.

1.2 Objectives

The goals of this thesis will be to design and construct a prototype of a haptic feedback joystick that can provide a torque feedback. What a reasonable torque feedback is will also be evaluated in this thesis. In order to verify the usefulness of the joystick, a model of a vehicle will be created so that the behaviour can be estimated and used for haptic feedback. The objectives are broken down into subtasks shown below.

- Joystick prototype
- Haptic feedback
  - Tracking
  - Mechanical stop
  - Centring
  - Friction
- Simulation of vehicle for testing

1.3 Delimitations

Working with haptic feedback implementation into vehicles is a project that can be extended to encompass a vastly complex model with estimations for rubber types in the wheel and different ground conditions. The joystick itself can also be constructed in numerous ways, for example the number of dimensions etcetera. All that work is outside the scope of this thesis, therefore this thesis will only produce one type of joystick with haptic feedback in only one dimension, namely the left and right dimension for steering.

The second delimitation is the model of the vehicle, which will be a simplified model in only two dimensions, removing changes in elevation. Some other simplifications will be made and will be presented in the modelling chapter. Presented as bullet points these delimitations can be seen below.

- 1-dimensional joystick
- Basic dynamic vehicle model
- Vehicle modelling in two dimensions

1.4 Thesis Outline

Introduction will be followed by a theory chapter where the different modelling techniques and the control theory used will be presented. This chapter will also contain an analysis of previous works. The next chapter will describe the hardware and the parts used for the joystick. The following chapter is the modelling part which will be separated into joystick modelling and vehicle modelling. The chapter will also include some delimitations of the vehicle model. Afterwards follows the chapter about controllers, both the design for the vehicle and the joystick. In the same chapter the implementation of the controllers and the model on the hardware will also be described. Results will follow this and lastly the discussion and conclusion will present an analysis of the result and recommended future work.

2

Theory

The theory chapter will concern the previous works in this field, for example truck and trailer modelling, haptic feedback devices such as steering wheels and tactile pen-devices. As well as describe modelling methods for dynamic systems and control theory for tracking and haptic feedback.

2.1 Previous Work

The project is divided into two main parts, one being the vehicle modelling and the second the joystick construction and control. The joystick can in turn be divided into hardware and control. Thus three different sources of information will be treated in order to cover these topics.

The vehicle modelling field is extensive, throughout the years a lot of development has been made. Particularly in the field of autonomous vehicles where the exact position and velocity can be crucial. In the case of articulated vehicles most work found has been done for trucks with trailers or mining vehicles, an example is the work of *P. Nyman, K. Uhlén* [7]. In the work mentioned the task is to control the joints, often referred to as waists, in long heavy vehicles, freight trucks with additional trailers. Their method for the modelling is *Euler-Lagrange* with generalised coordinates compared with basic newton formulas for movement. The same method is used by *Chen, C. Tomizuka, M.* in [8].

Some works also discuss wheel loader type construction equipment vehicles, mainly in the mining industry because of the hazardous environments that the vehicles operate in where autonomous vehicles would improve working conditions. These vehicles are often referred to as Load Haul Dump (LHD) vehicles, see figure 2.1. This type of mining vehicle closely resembles a wheel loader. The vehicles have a low profile to be able to operate in low ceiling tunnels. In the works of *Dragt, J.* [9] the focus lies on the

Figure 2.1: Example of a LHD used in mining operations. Picture borrowed from [9].

modelling of said mining vehicle for autonomous control. The main issue there was to find a reliable tyre model to represent the real movement. Since they did not compare with any real measurements it is not clear how well the model represented the real world LHD vehicle. The modelling of the dynamics was made by using *Euler-Lagrange* theory. This type of modelling represent the kinetic and potential energies in relation to a chosen set of coordinates, referred to as generalised coordinates, according to the principle of *D'Alembert*. This is useful as it focuses the modelling around this set of coordinates instead of setting up the reaction forces for the whole model. Focus of haptic feedback devices has previously been on remote control machinery, gaming devices and aircraft controls [10]. The latter is one of the first industries to use SBW or Fly-By-Wire (FBW). Among the first aircraft manufactures to implement this feature was Airbus with the A320, seen in figure 2.2 [11]. The use of FBW allows for an unstable design of the aircraft and this can improve weight and costs [4].

In the works of *Gil, J. J. et al 2013* [13] the haptic feedback device is a one dimensional joystick with a motorbike throttle for acceleration. The main haptic feedback for steering in that work was defined by three parameters, a gain proportional to the angle of the joystick that simulates a spring, an angular velocity based dampening effect and lastly a gain proportional to the angular error between the vehicle and the joystick. The evaluation was made against a conventional steering wheel with a similar haptic feedback. The results showed that the steering of the vehicle with the haptic feedback device was intuitive and provided a natural feel. However, the handling of the haptic feedback device closely resembles that of steering with a conventional steering wheel, also the test was compared with another SBW device and not a real car. Another haptic feedback device is the tactile pen-formed device that can be used to simulate a scalpel or a pen.

Figure 2.2: Airbus - A320. Picture borrowed from [12].

A work using this type of device is another work of *Gil, J. J. et al 2014* [14], this work used an *Impedance* controller, which allows for a penetration of the object that is sensed. The controller type is not as aggressive as for example a *proportional-integral* (PI), controller. Another work that included a pen-based sensory device is the works of *K. Kuchenbecker et al.* Their goal was to imitate impact on wood, by tapping with a pen shaped haptic feedback device. According to their research a human operator can only get limited knowledge of the stiffness of a surface when pressing down slowly, to get a deeper knowledge the person would have to tap on the surface. The reason behind this is that the human body can sense high frequency responses while only exert low frequency impulses. This is why the tapping is important when sensing a surface. Therefore, any device only capable of representing the low frequency behaviour will only provide a haptic feedback of limited usefulness. One of their conclusions was that a *proportional impact* controller would never be able to realistically imitate a stiff surface due to the high demand on the update frequency. They used a combination of closed loop and open loop to simulate the complex feeling of tapping on a stiff surface. The reason behind this is that the low frequency resisting force can be modelled by a gain proportional to the impact depth and the high frequency can be modelled as a decaying high frequency sinusoidal impulse response. The high frequency could be several 100 Hz. Their solution was to use a closed loop static gain for the low frequency response and an open loop event based transient response. The latter used measured impact responses as a base which was scaled by magnitude to meet the impact momentum of the haptic feedback device. The result was that the movement was stopped by the high frequency open loop controller and later maintained by the low frequency *proportional* controller.

2.2 Modelling

The main reason for modelling is to provide a platform for testing without having to build a prototype. This can then be done in numerous ways and levels of precision, everything from a drawn sketch of the vehicle to a fully parametrised model of the vehicle can be considered as a model. The usefulness of the model depends on the task at hand, the first sketch might be useful when a new design is being developed or a new part is supposed to be attached to the vehicle. The second is a mathematical model of the vehicle which is useful when for example an autonomous vehicle is being developed. In the autonomous case it is important to have as accurate movement and behaviour as possible in order to estimate the position of the vehicle.

In this chapter the modelling theories used will be explained as well as compared with other works. For the vehicle the important aspect is the angle tracking, the vehicle should behave as close to a real vehicle with respect to the steering, while the exact position and motor torque is considered to be of low priority.

The vehicle will be modelled by using the dynamic *Euler-Lagrange* in combination with the notion of virtual work, *D'Alembert's principle*, applied as generalised forces.

2.2.1 Euler-Lagrange

The *Euler-Lagrange* method uses energies as a balance equation. The *Euler-Lagrange* equation consists of the potential and kinetic energy, T and V. These together form the Lagrangian, denoted with L in the following equation. $L = T - V$ [15].

$$\frac{d}{dt}\frac{\partial(L)}{\partial(q)} - \frac{\partial(L)}{\partial(\dot{q})} = 0. \tag{2.1}$$

Where L in its general form is the following with m_i and J_i as masses and moments of inertia, v_i velocities, ω_i as angular velocities and h_i as vertical displacements. The i denotes the particles that makes up the system, and g is the gravitational constant.

$$L = T - V = \frac{1}{2}m_i v_i^2 + \frac{1}{2}J_i\omega_i^2 - m_i g h_i,\ i = 1...n$$

2.2.2 D'Alemberts Principle

The *D'Alembert's* principle introduces the concept of virtual work applied through forces F_i and moments that acts on a system of n particles [15]. The virtual work δW associated with masses m_i is shown below,

$$\delta W = \sum_{i=1}^{n}(F_i - m_i a_i)\delta r_i, \tag{2.2}$$

a_i is the acceleration and δr_i is the virtual displacement of the masses. This in turn can be expressed as generalised coordinate forces. *D'Alembert* showed that with a system

in equilibrium, where the sum of the added forces and the inertial forces are zero, the virtual work done to the system can be expressed as the following.

$$\delta W = (Q_j - Q_j^*) * \delta q_j = 0, j = 1...m,$$

where q_j are the generalised coordinates as seen in the above equation, for every generalised coordinate there is a set of forces $Q_j - Q_j^*$ which all sum up to zero. Where Q_j^* are the inertial forces and Q_j the added forces, these can then be written in a familiar form,

$$\frac{d}{dt}\frac{\partial T}{\partial q} - \frac{\partial T}{\partial \dot{q}} = Q_j.$$

T in the equation is the kinetic energy in a system of rigid bodies. Looking at equation 4.8, this is also the equation when V, the potential energy, is zero. Therefore the resulting equation for the system in dynamic equilibrium is,

$$\frac{d}{dt}\frac{\partial L}{\partial q} - \frac{\partial L}{\partial \dot{q}} = Q_j. \tag{2.3}$$

2.3 Haptic Feedback & Control

The objectives for the haptic feedback joystick states there should be a simulated mechanical stop to simulate maximum turn angle as well as a spring centring and an angle tracking behaviour related to the error between the vehicle and the joystick, a velocity dependent friction component will also be added. This could be done with numerous types of controllers, cascaded or implemented as one. Model Predictive Control (MPC) would for example be able to handle all these objectives. The drawback would be the requirements on the model and the computing power. Another solution is to use a *Proportional-Integral-Derivative* (PID) type controller. One way to use this is to create a cascaded version of a P controller and a PI or a *Linear Quadratic Regulator* (LQR) controller for the angle tracking [16]. A possible improvement of the P and PI controller is to have a varying proportional gain, for example when the error approaches zero the gain could become larger. The LQR controller is in essence a P controller that regulates on all states instead of just one, this means that several references could be used at the same time.

2.3.1 PID

The PID controller is the most common type of controller [16]. The standard form looks as follows,

$$u = P \cdot e(\tau) + I \int_0^t e(\tau) d\tau + D \frac{d}{dt} e(\tau),$$

where $e(\tau)$ is the error between the reference and the output from the system, u is the control signal fed to the system, P is the proportional gain, I is the integral gain and

D is the derivative gain. The controller is rather simple to tune manually and there exists a lot of software to tune it automatically, one example is the auto-tune function in MATLAB Simulink [17].

2.3.2 LQR

The LQR is a controller that can be used for a Multiple Input Multiple Output (MIMO) system as in the following equation,

$$\begin{aligned} \dot{x} &= Ax + Bu \\ y &= Cx + Du \end{aligned}$$

where x is the state vector, u is the control signal, A is the *dynamics matrix*, B is the *control matrix*, C is the *sensor matrix* and D is the *direct term*. y is the output vector. The controller minimises a cost function J.

$$J = \int_0^\infty x^T Q_{wx} x + u^T Q_{wu} u \; dt, \tag{2.4}$$

where $Q_{wx} \geq 0$ and $Q_{wu} \geq 0$ are positive semi definite symmetric matrices. The minimisation is a trade-off relation between the control signal u and the size of the error from the origin regarding the states x. Choosing Q_{wx} and Q_{wu} is therefore dependent on the importance of the tracking versus the stability of the control signal. A standard simple choice of the matrices is to use diagonal weights, The weights corresponds to each state and control signal, by making a certain weight larger that states importance is higher and vice verse. Making the weights on Q_{wu} large signifies that the change of control signal should be penalised. The matrices in diagonal form are shown below.

$$\mathrm{Q}_{wx} = \begin{pmatrix} q_1 & & 0 \\ & \ddots & \\ 0 & & q_n \end{pmatrix} \qquad \mathrm{Q}_{wu} = \begin{pmatrix} p_1 & & 0 \\ & \ddots & \\ 0 & & p_n \end{pmatrix}$$

The control law for the LQR is of the form

$$u = -Q_{wu}^{-1} B^T P x,$$

where P is the solution that satisfies the following *Algebraic Riccati equation*,

$$PA + A^T P - PBQ_{wu}^{-1} B^T P + Q_{wx} = 0$$

The control law is usually written as

$$u = -Kx.$$

Where K is the feedback gain seen in figure 2.3, the control signal is then fed back to the system.

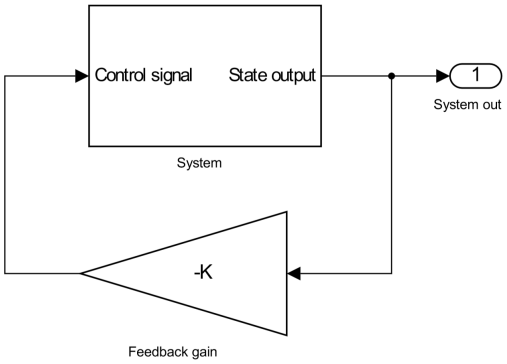

Figure 2.3: LQR scheme with reference set to zero

2.3.3 LQI

For the LQR to achieve error free tracking the model has to be accurate, when there are uncertainties or when an inaccurate model is not possible to achieve, there is another solution to reach the correct steady state. This method is to add an integral action to the LQR, thus removing any steady state errors. The process is done by adding a new state to the state space, the new state, z, is the error between the references, r, and the states. The update equation for the new state is as follows,

$$\dot{z} = Cx - r.$$

This in turn creates a new state space that looks as follows

$$\begin{bmatrix} \dot{x} \\ \dot{z} \end{bmatrix} = \begin{bmatrix} A & 0 \\ C & 0 \end{bmatrix} \begin{bmatrix} x \\ z \end{bmatrix} + \begin{bmatrix} B & 0 \\ 0 & -1 \end{bmatrix} \begin{bmatrix} u \\ r \end{bmatrix}$$

$$y = \begin{bmatrix} C & 0 \end{bmatrix} \begin{bmatrix} x \\ z \end{bmatrix} + Du.$$

From this new state space the LQR gain K is calculated as the process described previously and the new control signal will be $u = Kx + K_i z$. The new block system looks as in figure 2.4 [16].

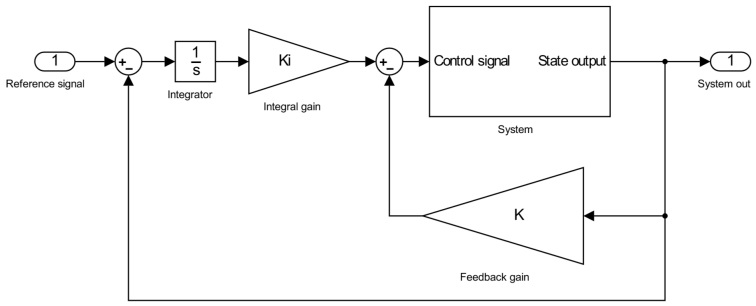

Figure 2.4: LQI scheme with reference signal

2.3.4 Event Based Haptic Feedback

In order to construct the event based controller discussed in [10], some measurements should be made to establish the frequency of the impact deceleration. These can be made by measuring the acceleration when hitting the object intended for simulation, i.e. moving the joystick at a constant speed into a mechanical stop and measuring the acceleration. The measurement should be done for a set of different angular velocities to get a good set of velocity based amplitudes for the impact response.

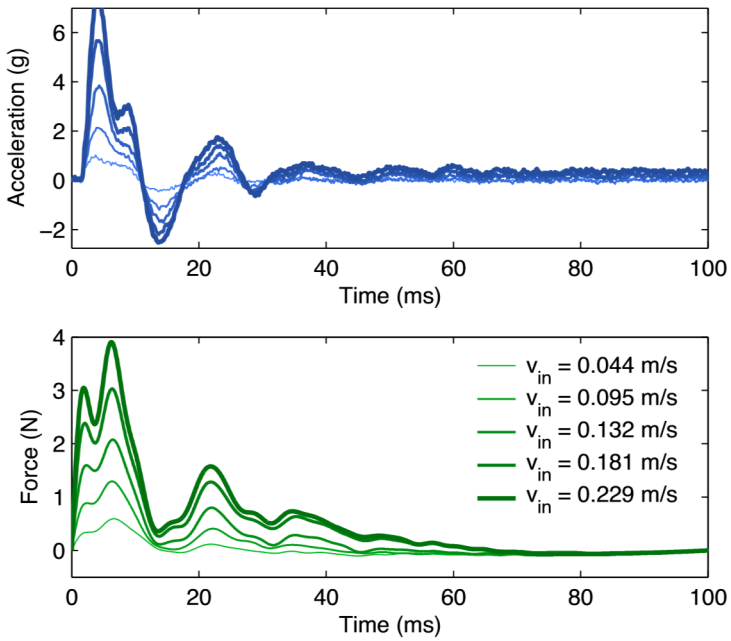

Figure 2.5: Impact response with acceleration and force, borrowed from [10]

In figure 2.5 the result from the measurement done by *K. Kuchenbecker et al.* [10] can be seen, where the different lines in the figure represent the different attack velocities. To imitate a full stop the upper curve must be simulated and sent as a counter effect. The equation for the countering force, simulating the decaying sinusoid seen in the upper plot follows,

$$F_{sin} = A|v_{in}|e^{\ln(0.01)t/d}\sin(2\pi ft) \ for\ 0 < t \leq d, \tag{2.5}$$

where A is the amplitude, v_{in} is the velocity at impact, t the time from impact, d is the stop time for the sinusoid and lastly f is the frequency. A is tuned to provide a force that feels passive, yet stops the motion according to the specific material used for the mechanical stop. The amplitude is scaled by the incoming velocity to provide a reasonable resisting force, the length of the sinusoid relates to the inertia of the system, a high inertia would provide a slower system. For the case with a wooden surface the frequency of the system was measured to 55 Hz and the duration to 0.055 s [10].

In order to fully stop the haptic feedback device at the simulated end a controller that keeps the force to prevent any further penetration of the object is needed. This will be done by a proportional gain of the form seen in the following equation,

$$F_{prop} = \begin{cases} -Kx, & x > 0 \\ 0, & x \leq 0, \end{cases} \tag{2.6}$$

where $x = 0$ is the position of the surface, positive direction into the object, and K is the proportional gain.

3

Hardware

To evaluate different controllers and their benefits when it comes to haptic feedback, the actual feel must be evaluated. To do this, a platform is needed that fulfils the requirements needed to evaluate the haptic feedback. There were no commercial units that meet the requirements so a platform was constructed by mostly off the shelf components. This chapter describes the hardware parts used in this thesis, and how they were assembled and the test rig for estimation the torque needed for a simulated mechanical stop.

3.1 Micro Controller

To be able to calculate the different outputs and read the sensors a micro controller was needed. The Arduino DUE was picked for it's relatively fast CPU, adequate numbers of I/O ports and the ability to use a 12 bits A/D converter. A full description of the Arduino DUE hardware can be found on the Arduino homepage [2].

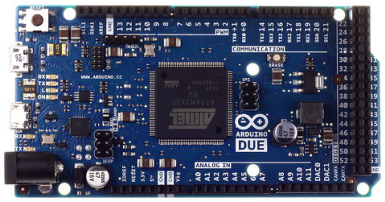

Figure 3.1: Arduino DUE. This picture is borrowed from [2].

3.2 Actuator

To minimise the time used for construction, an existing gearbox with two attached DC motors were extracted from a force feedback steering wheel made for computer gaming.

The two DC motors was connected to the same gear which in turn was mounted directly to the steering shaft.

3.2.1 Gearbox

The ratio between the motor and the shaft was approximately 16:1. The gearbox only had one gearwheel, which had helical gears. The gearwheel itself was made up of two identical gearwheels, side by side with the same shaft, held together by a spring. The spring pulls the two gearwheels towards each other and force the gearwheels to connect with the gears on to the motors. This minimises the backlash caused by the gearbox which is an undesirable phenomenon when it comes to haptic feedback.

3.2.2 DC Motors

The DC motors attached to the gearbox was of the model RS-555SH-15260. These motors have a nominal voltage of 24 V, stall current of 0.72 A and a stall torque of approximately 0.085 Nm. More information about these motors can be found in the datasheet in appendix C.

3.3 Motor Controller

The original motor controller for the force feedback steering wheel which the gearbox and motors were extracted from could not be used in this thesis, another motor controller had to be obtained. Measurements on the original setup indicated that when working at full torque, a maximum of approximately 24 V and 1 A was measured. The VMA03 motor shield (seen in figure 3.2) from *Velleman* was considered sufficient since it was capable of providing up to 50 V with 2 A by a PWM signal. More information about this motor controller can be found in appendix E.

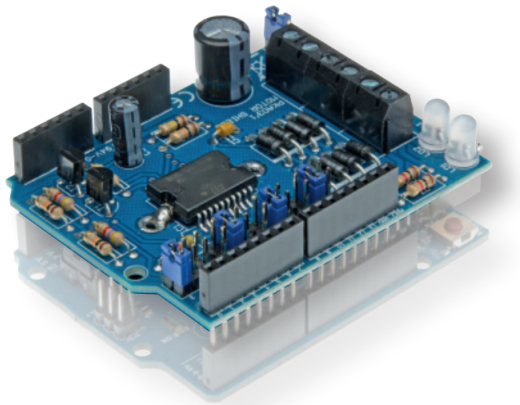

Figure 3.2: The VMA03 motor shield from *Velleman*. Picture borrowed from [18].

A drawback with the VMA03, was that the communication ports were rated to 5 V and the output from the Arduino DUE in 3.3 V. This meant that the signals had to be amplified if this motor shield was going to work properly. The solution was to add a level shifter, a level shifter can amplify from one voltage domain to another. In this case from 3.3 V to 5 V. The level shifter selected for this task can be found in appendix D.

3.4 Handle

As a handle to the platform, a discarded joystick from an actual articulated vehicle was used. This handle could not be directly mounted to the gearbox, a custom part had to be constructed for this purpose. The resulting part with the handle can be seen in figure 3.3.

Figure 3.3: The handle used in this thesis.

3.5 Sensors

For the controllers the angle, angular velocity and current had to be provided, either by estimation or measuring the actual states. This section describes how these states were derived.

3.5.1 Angle

By mounting a potentiometer on the gearbox and measuring the voltage drop over the resistance a relative angle could be obtained. The potentiometer used was the 91A2A-B28-B15 from *Bourns*, which contains two linear resistances at 10 kΩ with a single turn.

Since reading the analog ports of the micro controller could be executed at a higher

rate than the main operation, these sensors were sampled 10 times faster than the main loop. These samples were then filtered by a basic median filter, which could remove potential spikes and some high frequency noise. The angle from this method of sampling resulted in low level of noise and with no filtering delays. Read more about this potentiometer in appendix B.

3.5.2 Angular Velocity

Due to the fact that the level of noise was relatively low when measuring the angle and filtered out short lived spikes, the angular velocity was derived from the measured angle using a discrete derivation,

$$\frac{(z-1)}{T_s z},$$

where z is the Z-transform and T_s is the time step.

3.5.3 Current

To be able to get an estimation of the applied torque from the motors, the current was selected to be measured. To measure the current the current sensor ACS712 from *Allegro* was used, which is a hall effect-based linear current sensor. Unlike the measurements from the angle, this signal was influenced by a relatively high level noise. To suppress the noise, a digital low-pass filter was designed using Simulink.

3.6 Assembly

The components were assembled on an aluminium frame, which was convenient when testing and transporting the rig. Using two clamps, the frame could be fixed on a table when in use. The motor controller was powered by an external power supply. The complete setup can be seen in figure 3.4.

3.7 Output Verification

Estimating

To be able to simulate a mechanical stop, the amount of torque needed must be estimated in order to get a benchmark. In order to measure the torque needed, a test rig was made by using a scale fastened to a lever. This scale would be used to measure the applied force (F), which was used to calculate the torque (τ) through equation

$$\tau = r \times F,$$

by using the known length (r) of the joystick. Using this method the approximately torque needed to simulate a mechanical stop was found to be 2.5 Nm. This torque was large enough to hinder any further movement, moving the lever beyond this required an uncomfortable amount of force.

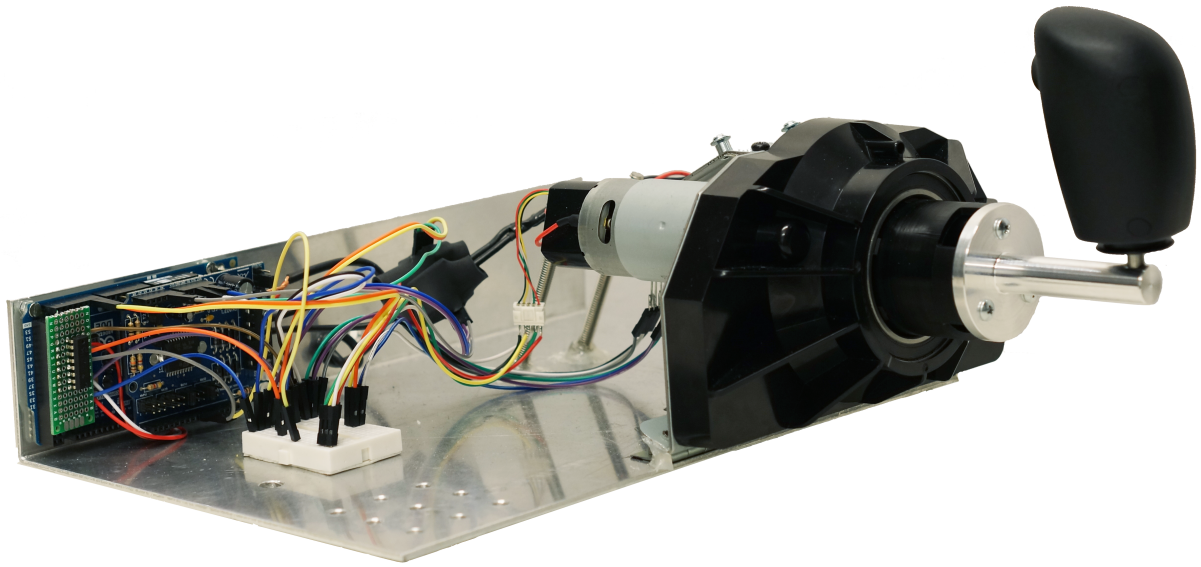

Figure 3.4: The assembly.

Verification

According to the datasheet, the motor can provide a maximum of approximately 0.085 Nm. Both of them can generate 0.170 Nm, and with a gearbox ratio of 1:16, the resulting torque applied to the joystick shaft will be approximately 2.7 Nm. Theoretically, this is enough to simulate the mechanical stop.

4

Modelling

For the modelling of the vehicle a set of different steps will be evaluated for the final models. First of all the joystick and the vehicle will be separated into two models. The joystick will be modelled in Simscape, a MATLAB toolbox for modelling real world applications using sub categories in electronics, mechanics etcetera. The complexity of the vehicle however will be handled by breaking it down into a simpler model with two point masses and inertias. Thereafter the vehicle will be modelled both by kinematic expressions of velocities and angles as well as dynamic representation with Euler-Lagrange coupled with forces.

4.1 Vehicle

As stated earlier an articulated vehicle will be modelled, namely a wheel loader seen in figure 4.1.

4.1.1 Delimitation

The purpose of the vehicle model is to provide a simulation platform for testing the joystick, therefore it is not critical to maintain an accurate model in the sense of tracking. Since the exact position is irrelevant the effects of slip can be neglected. The vehicle will be modelled as a modified bicycle model, meaning that the vehicle will only have two wheels and therefore it will only have two points of attack for the tyre forces.

4.1.2 Kinematic Model

The basic representation of a vehicle is the kinematic representation, it is composed by using velocities and rotations to express the heading of the vehicle. First off is the modified bicycle model with velocity V. These can be transformed to components in x

Figure 4.1: Articulated vehicle.

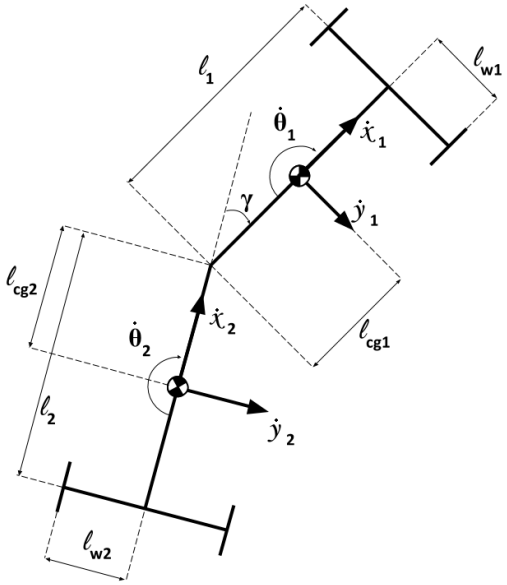

Figure 4.2: Sketch of vehicle with forces and velocities.

and y as well as rotational velocity $\dot{\theta}$ by utilising the steering angle γ as seen below,

$$\dot{x} = V\cos\theta, \tag{4.1}$$
$$\dot{y} = V\sin\theta, \tag{4.2}$$
$$\dot{\theta} = V\frac{\tan\frac{\gamma}{2}}{L}. \tag{4.3}$$

For the articulated vehicle the model must be modified slightly to take into account the two parts of the vehicle, this will be done in the same way as done by *Lilja, R* in [19]. As

can be seen in the following equations the vehicle now has two rotational components, $\dot{\theta}_1$ and $\dot{\theta}_2$. The lengths l_1 and l_2 can be found in figure 4.2.

$$\dot{x}_i = V\cos\theta_i, \tag{4.4}$$

$$\dot{y}_i = V\sin\theta_i, \tag{4.5}$$

$$\dot{\theta}_1 = V\frac{\sin\gamma}{l_2+l_1\cos\gamma}+\dot{\gamma}\frac{l_2}{l_2+l_1\cos\gamma}, \tag{4.6}$$

$$\dot{\theta}_2 = V\frac{\sin\gamma}{l_2+l_1\cos\gamma}-\dot{\gamma}\frac{l_2\cos\gamma}{l_2+l_1\cos\gamma}. \tag{4.7}$$

This type of model works well for low velocities where slip and dynamic behaviour is not needed. However, since the model has to include dynamic behaviour in order to behave realistic when controlled by the joystick, a more advanced model is needed.

4.1.3 Euler-Lagrange

The *Euler-Lagrange* equation is stated below in equation (4.8) as in the theory chapter, in this case an assumption is made that the vehicle will not move vertically. This gives us the possibility to remove the potential energy, in other words, $V = 0$.

$$\frac{d}{dt}\frac{\partial(L)}{\partial(q)}-\frac{\partial(L)}{\partial(\dot{q})}=0. \tag{4.8}$$

The potential energy being zero leaves only the kinetic energy, well known as,

$$L=\frac{1}{2}m_i v_i^2+\frac{1}{2}J_i\dot{\theta}_i^2, \tag{4.9}$$

where $i = 1,2$ and represents the front and the rear unit of the vehicle, m_i is the mass, J_i the moment of inertia and v_i and $\dot{\theta}_i$ are planar velocities and angular velocities respectively. The velocities and rotations will be expressed in reference to the centre of gravity of the front unit. This means that the forward velocity has components, $\dot{x}$ and $\dot{y}$ as follows,

$$v_1=\sqrt{\dot{x_1}^2+\dot{y_1}^2}.$$

The rear unit is influenced also by the angular velocity of the front and rear unit, $\dot{\theta}_1$ and $\dot{\theta}_2$. The latter is expressed by a relation between the articulation angle and the rotational angle around the centre of gravity of the front.

$$\theta_2=\theta_1-\gamma. \tag{4.10}$$

The velocity of the rear will be as follows,

$$v_2=\sqrt{\dot{x}_2^2+\dot{y}_2^2},$$

where $\dot{x}_2$ and $\dot{y}_2$ are the following

$$\begin{aligned}\dot{x}_2 &= \dot{x_1}\cos\gamma + (\dot{y_1} - l_{cg1}\dot{\theta_1})\sin\gamma, \\ \dot{y}_2 &= -\dot{x_1}\sin\gamma + (\dot{y_1} - l_{cg1}\dot{\theta_1})\cos\gamma - l_{cg2}(\dot{\theta_1} - \dot{\gamma}).\end{aligned}$$

4.1.4 Derivation of equations

The next step is to connect the Lagrangian to the generalised forces. The model will be constructed in the same way as in the works of *He, Qichang et al.* [20]. The coordinates that will be used in the dynamic model can be derived from figure 4.2. The dynamic model will use the front unit as reference point and therefore the forces that will be used are in connection to the front centre of gravity. Those are longitudinal, lateral and rotational, x_1, y_1, θ_1 and the moment around the joint related to the front unit, M_1.

$$\frac{d}{dt}\frac{\partial L}{\partial \dot{x_1}} - \frac{\partial L}{\partial x_1} = Q_{x_1} \tag{4.11}$$

$$\frac{d}{dt}\frac{\partial L}{\partial \dot{y_1}} - \frac{\partial L}{\partial y_1} = Q_{y_1} \tag{4.12}$$

$$\frac{d}{dt}\frac{\partial L}{\partial \dot{\theta_1}} - \frac{\partial L}{\partial \theta_1} = Q_{\theta_1} \tag{4.13}$$

$$\frac{d}{dt}\frac{\partial L}{\partial \dot{\gamma}} - \frac{\partial L}{\partial \gamma} = Q_{\gamma} \tag{4.14}$$

Using equation (4.9) we can from (4.11)-(4.14) derive the nonlinear set of equations seen in equation (4.15) to (4.18). Where the left hand side represent the generalised forces in the coordinates of the above stated equations. In order to put the system on a state-space form with the highest order derivatives separated from the equations it has to be represented as a descriptor system seen in equation (4.19).

$$F_{x1} = (m_1 + m_2)\cdot\ddot{x}_1 + m_2 l_{cg2}\sin\gamma\cdot(\ddot{\theta}_1 - \ddot{\gamma}) + m_2 l_{cg2}\cos\gamma\cdot(\dot{\theta}_1 - \dot{\gamma})\dot{\gamma}, \tag{4.15}$$

$$F_{y1} = (m_1 + m_2)\cdot\ddot{y}_1 - m_2 l_{cg2}\cos\gamma\cdot(\ddot{\theta}_1 - \ddot{\gamma}) + m_2 l_{cg2}\sin\gamma\cdot(\dot{\theta}_1 - \dot{\gamma})\dot{\gamma}, \tag{4.16}$$

$$\begin{aligned}M_{\theta}1 = {} & (I_1 + I_2)\cdot\ddot{\theta}_1 - I_2\ddot{\gamma} + m_2 l_{cg2}^2\cdot(\ddot{\theta}_1 - \ddot{\gamma}) + m_2 l_{cg2}^2\ddot{\theta}_1 + 2m_2 l_{cg1} l_{cg2}\cos\gamma\cdot\ddot{\theta}_1 \\ & ... + m_2 l_{cg2}\sin\gamma\cdot\ddot{x}_1 - m_2 l_{cg1}\ddot{y}_1 - m_2 l_{cg2}\cdot(\ddot{y}_1 + l_{cg1}\ddot{\gamma}) + m_2 l_{cg2}\dot{\gamma}\cos\gamma\cdot\dot{x}_1 \\ & ... - 2m_2 l_{cg1} l_{cg2}\dot{\gamma}\sin\gamma\cdot\dot{\theta}_1 + m_2 l_{cg2}\dot{\gamma}\sin\gamma\cdot(\dot{y}_1 + l_{cg1}\dot{\gamma}),\end{aligned} \tag{4.17}$$

$$\begin{aligned}M_{\gamma} = {} & I_2(\ddot{\gamma} - \ddot{\theta}_1) + m_2 l_{cg2}^2(\ddot{\gamma} - \ddot{\theta}_1) - m_2 ł_{cg2}\cos\gamma\cdot(l_{cg1}\ddot{\theta}_1 - \ddot{y}_1) \\ & ... + m_2 ł_{cg2}\dot{\gamma}\sin\gamma\cdot(l_{cg1}\dot{\theta}_1 - \dot{y}_1) - m_2 ł_{cg2}\sin\gamma\cdot\ddot{x}_1 - m_2 ł_{cg2}\dot{\gamma}\cos\gamma\cdot\dot{x}_1.\end{aligned} \tag{4.18}$$

$$E\cdot\ddot{x} = F + H(x,\dot{x}) \tag{4.19}$$

E is the matrix containing the dynamics related to the states, F the generalised forces while H is the dynamics related to x and $\dot{x}$. F and H are vectors with the same dimension as the x vector.

The equation can be rewritten as a state space representation:

$$\ddot{x} = E^{-1}F + E^{-1}H(x,\dot{x})$$

The $\ddot{x}$ vector contains the accelerations in x and y direction, $\ddot{x}_1$ and $\ddot{y}_1$ as well as the angular acceleration of the front $\ddot{\theta}_1$ and waist of the vehicle $\ddot{\gamma}$.

4.1.5 Generalised Forces

As seen in the above equation the forces are represented as a net force in each direction. The forces in each coordinate is the summation of the forces and moments concerned with each point. The vehicle will be treated as a bicycle much like the works of *He, Qichang et al.* [20]. The wheel forces will therefore be centred in the joint of the wheel axle and the vehicle centre line. The forces are then split into longitudinal and lateral directions as in the *Lagrange* equations, F_{x_1} and F_{y_1} where the number 1 signifies that the forces are at the front of the vehicle. The moments are centred around the front centre of gravity M_{θ_1} and the waist of the vehicle M_γ.

4.2 Joystick

The joystick is as mentioned in the introduction and the hardware section a one dimensional joystick with a gearbox attached, it can be seen in figure 4.3.

Figure 4.3: Handle with gearbox

4.2.1 Delimitation

Since the hardware was not going to be altered after assembly, no future editing of the model after its be derived would be needed. Therefore a Simscape model with greybox

estimation of unknown parameters was considered to be sufficient for this task. This method was also considered faster to complete than a manually derived dynamic model. The measurements needed for the estimation was done using the hardware itself with the exception for the angular velocity. The angular velocity was measured using an optical encoder which was not used later on in the project. The reason why the optical encoder was used during the estimation was because this method enabled the joystick to do multiple turns instead of the fixed span of the potentiometer, which the final version used later could not.

4.2.2 Simscape Model

Since the Simscape environment have build-in blocks for DC motors which only need information provided by the datasheet, the parameters that would need to be estimated involved friction and inertia from the gearbox. To capture these parts a series of measurements were conducted which included step responses, increasing and decreasing ramps and sinusoidal inputs. The model of the joystick with both motors can be seen in figure 4.4

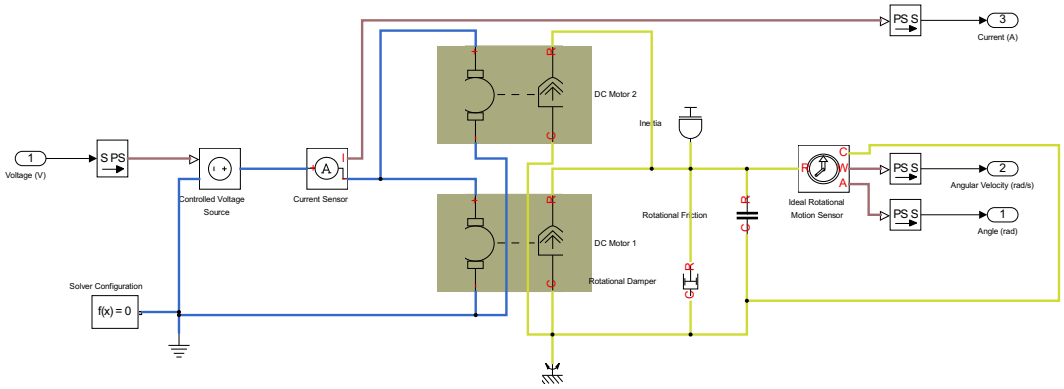

Figure 4.4: Simscape model of the joystick used for parameter estimation

The measurements was then used to estimate the unknowns using another Simulink toolbox called *Simulink Design Optimization*. Using this tool the parameters was estimated and used in to the Simscape model. A comparison between a measurement and the Simscape model can be seen in figure 4.5.

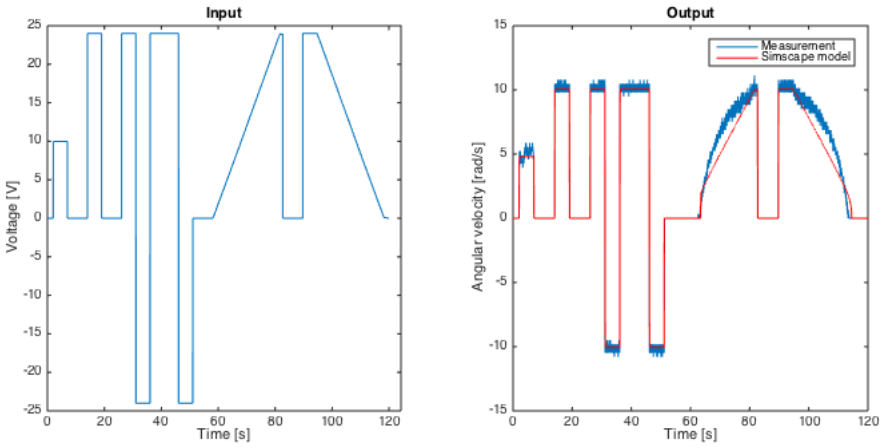

Figure 4.5: Measurement using the optical encoder in comparison with the output from the Simscape model

5

Controllers

The theory chapter states some types of controllers used in this thesis, those are PID and LQR types of controllers as well as the event based open loop controller. Variants of these were combined in order to meet the required performance. For the vehicle control a type of LQR with an integrating part, a so called LQI controller was used. The choice motivated by the demands on tracking of the angle, no steady state error was acceptable. For the joystick, the controllers performance was of a more subjective manner. In order to fully simulate the mechanical connection between the joystick and the vehicle a set of different tasks was set up as objectives. These were the tracking, the centring, the simulated mechanical stop and the friction. For the mechanical stop a solution similar to the method used by *K. Kuchenbecker et al.* [10], with event based open loop control was used. This can be coupled with speed dampening terms as in the PD controller.

5.1 Design of Controllers

The design of controllers can follow a different set of steps. A methodical approach is to create a model and work from that to establish a stabilising controller. This way was used on the vehicle and the angle tracking part of the joystick. There the model was linearised and the state space was used for calculation of the state feedback gain. However all of the controllers needed fine tuning to cope with the fact that the haptic feedback is subjective and could be hard to measure.

5.1.1 Joystick

The controller of the joystick has a major task and several subtasks to carry out as mentioned earlier. The foremost objective is to provide a haptic feedback. This behaviour can be broken down into several different tasks, tracking, centring, simulated mechanical stop and friction, those can be seen in the objectives section of the introduction. The centring force's purpose is to steer the vehicle into going straight. In order to make the

joystick move the voltage had to surpass a dead zone voltage, this puts demands on the controller to provide a control signal that is large enough.

Tracking

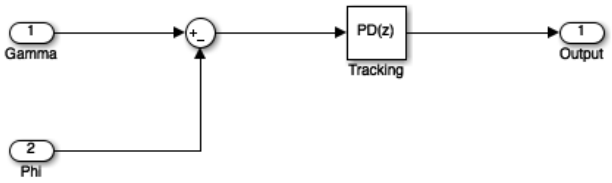

Figure 5.1: Tracking

Since the vehicle will act as the slave unit, following the joystick in this application, zero steady state tracking of the vehicle for the controller on the joystick side was considered unnecessary. The important behaviour of the joystick in relation to the vehicle is to hinder a too large deviation from the vehicle steering angle. This will be done by implementing a PD controller, the derivative acts on the rate of change of the angular error, this means that abrupt movements that the vehicle cannot follow will be hindered. The values was tuned using the pidtune in MATLAB and the joystick model, it was then manually tuned for the real plant using the pidtune values as a starting point. One of the issues is that the controller cannot be too aggressive, then the behaviour will feel stuttery, and if it is too slow the joystick will feel sluggish.

Centring

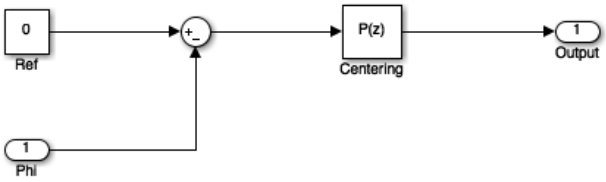

Figure 5.2: Centering

The goal for the centring force is to slowly straighten the vehicle, but if the operator is still holding the joystick the force must not increase as one should be able to turn for as long time as needed. Therefore an integrating part is not optimal as it would increase the force with time. A scheduled proportional gain was used for this task, the gain would increase when the absolute angle moved towards zero. As the error would decrease when closing to zero, a higher gain was needed to overcome the dead zone of the DC motors. The gain structure looks as follows, $P = p_0 + p_l \cdot |\phi|$, where p_0 is the base gain and p_l is the linear gain component.

Mechanical Stop

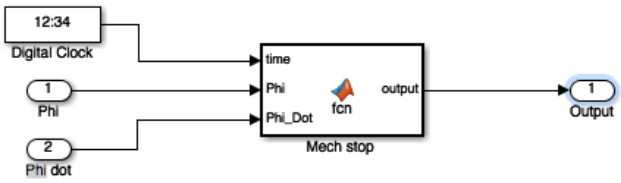

Figure 5.3: Mechanical stop

This task was to simulate a mechanical stop, which means that the stop should be sharp and strong. Any deviation beyond the specified angle should be penalised heavily. The main problem is to stop the incoming joystick abruptly and without considerable overshoot, afterwards it is possible to use a proportional gain to keep the resisting torque. The implementation of the event based controller according to the theory chapter required more time than available and would require a relatively noise free measurement of the acceleration, for example by using an accelerometer. Due to the time limitation and lack of such a sensor the impact reaction had to be manually tuned. As a starting point the same equation, equation (2.5) and values as used and presented in the theory chapter was used. These values were however deemed to create an unnecessarily sharp feeling since these parameters were for a pen hitting wood, a vehicle would behave differently. A tuning parameter that needed adaption was the duration of the sinusoid, since the mechanical device has higher inertia the total energy required to stop the joystick was higher than the impulse for the pen-device. Therefore the frequency had to be lowered and the amplitude increased in order to give a larger pulse for a longer duration. The frequency empirically determined to work well was 5 Hz with a duration of 0.4 s where the signal would in reality wear off at 0.35 s as can be seen in figure 5.4. The figure also includes several velocities at impact that are typical for normal operation. Where the original article used a current controller for the motors this project used as mentioned earlier a voltage based PWM controller, therefore the force was scaled to voltage by using the joystick model to determine which voltage gave the right amount of acceleration, this was one of the design factors of the amplitude of the sinusoid. Equation (2.6) describes this function. As in the theory section a regular P controller that activates whenever the impulse controller is activated was used to maintain the resisting torque.

Friction

The overall velocity of the joystick should also be dampened to restrict fast changes in the steering reference. The controller that suits this task is a P controller acting on the angular velocity. A speed dependency was added through changing the proportional gain according to the velocity of the vehicle. The faster the vehicle would go the more friction is added to prevent any sudden turns.

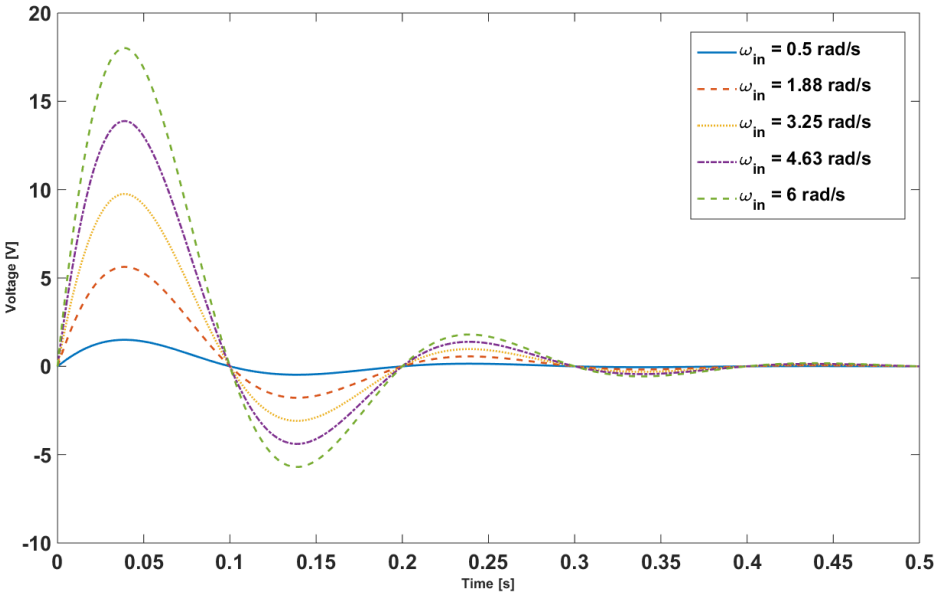

Figure 5.4: Voltage scaled impulse response for different impact velocities

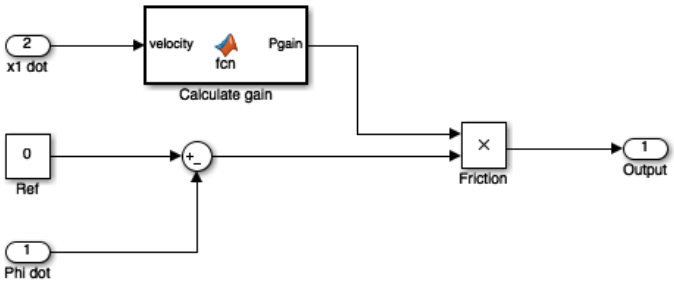

Figure 5.5: Friction

5.1.2 Vehicle

The vehicle takes both a velocity and an angle as reference input, this gives a Multiple Input Multiple Output (MISO) system, therefore a state feedback controller is used. As the theory chapter states, if the model includes some uncertainties or is not an exact model it is useful to implement a LQI controller for removal of any steady state error. This type of controller is used and both the velocity and steering angle states are augmented for the integrating part.

5.2 Implementation

This section briefly describes the implementation and visualisation of the controllers. Implementation in this section implies the process of getting the control algorithms to the hardware and visualisation implies the visual feedback to the user of how the vehicle is positioned.

5.2.1 Controller

The code was generated by using the Simulink support for running models on target hardware. Using this tool most standard blocks in the Simulink library and MATLAB scripts could be used for creating the control algorithms and sensors reading protocols.

To be able to set the Arduino DUEs analog read resolution to 12 bits instead of the default value of 10 bits, additional C/C++ code was needed. This was done by creating a S-block, a Simulink function block, which enabled the use of the Arduino library which in turned enabled the use of standard Arduino functions and methods.

5.2.2 Visualization

To be able to evaluate the haptic feedback, it became apparent that the user of the joystick would like a visual description of the position of the vehicle. Since the model was computed on the micro controller displaying the vehicle on a computer screen an interface was needed. A MATLAB GUI that communicated with the micro controller using a USB cable and plotted the vehicle was created for this task. The data transferred from the micro controller to the GUI, was the velocity and the angle of the vehicle. Using equation (4.4) to (4.7) and the output from the micro controller, the position and steering angle of the vehicle could be computed. Since this meant that a kinematic model was used to display a dynamic model, there were undesirable side effects. The back end would look like it would skid when the user turned sharply. This was considered to be an acceptable since this only occurred during extreme turning, which the haptic feedback controllers should hinder, and it was only a visual effect from the conversion. An example of a plot from the GUI is shown in figure 5.6.

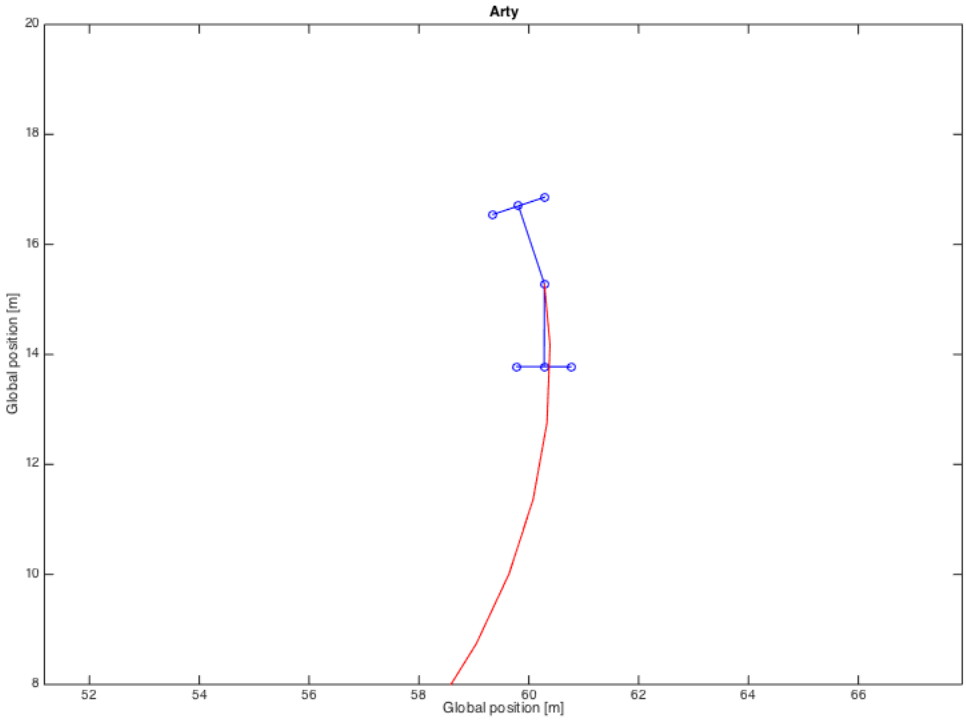

Figure 5.6: Example of the plotting of the vehicle in the MATLAB GUI where the plotted line is the historical positions of the joint.

6

Results

The goal of the thesis was to provide a haptic feedback solution with a joystick for an articulated vehicle. Brief considerations were made to investigate different solutions to find a feasible prototype, one was selected and from there on the haptic feedback and interface with the GUI was in focus. This chapter will present the results of the haptic feedback.

6.1 Haptic Feedback Feeling

This section is largely based on actual hands-on experience, which makes it less technical than traditional technical reports. A realistic haptic feedback is difficult to quantify and does not always relate to an accurate controller, therefore the comparison will be made by evaluating the controllers according to their comfortableness and functionality.

6.1.1 Complexity of Design

The PID category of controller is well known and the design method is well documented, it is a valid alternative for Single-Input-Single-Output (SISO) systems. Because it is a SISO controller the design is intuitive and easy to follow, one input leads to one output. Two PID controllers were used, one PD for angle and one P for angular velocity. The design was intuitive and made partly by utilising the auto tuned values with the help of the model. The event based controller needed some live testing to establish a working controller, even though the model was used to estimate the required voltage. The overall complexity when it comes to sensors was however low, since the event based controller was an open loop controller that only used the incoming velocity once per impact.

6.1.2 Tracking

The tracking of the joystick angle was made in order to prohibit the operator to move the joystick too far away from the vehicles steering angle. This type of compensation worked well to inform the user that the vehicle could not turn as fast as the user tried to. The overall performance felt realistic.

6.1.3 Mechanical Stop

Using the event-based controller to simulate the mechanical stop generated a convincing stop. The stop felt abrupt and sharp, but the user could move past the threshold by applying enough force, but that required a lot of effort and was far from comfortable for the user.

6.1.4 Centring

The centring worked as a weak spring fastened joystick with a built in damper. When released, the joystick would slowly raise itself towards the centre. The behaviour was a bit shaky due to the dead zone included in the motors and also due to the friction component which restricted movement. Since the gain would become smaller as the angle increased the force did not interfere with the normal control over the vehicle.

6.1.5 Friction

The simulated friction that would restrict the movement of the joystick felt smooth and realistic. This feature coincidentally supported the tracking, by prohibiting fast displacements of the joystick. The friction was scaled by the velocity of the vehicle, higher velocities would result in a higher resisting force.

7

Discussion and Conclusion

In this chapter the results and proposals of future work are discussed. This chapter also presents some problems that occurred during this thesis, which influenced the results and work.

7.1 Concluding Remarks

Event based haptic feedback has a great advantage over other closed loop control methods when it comes to simulating a mechanical stop. This is a similar conclusion as was derived in the works of *K. Kuchenbecker et al.* [10]. The haptic feedback can also be used to represent that the vehicle is hitting an object. For haptic feedback tracking, a PD controller worked better than a PI or PID since the latter two did not provide a realistic feeling, the resisting force in a haptic feedback device must be felt as a passive resistance, where a PI controller would be active and aggressive to movement. The PD controller gave a heavy response when the angular velocity was high and a softer resistance while moving the joystick at a normal rate.

[redacted][1]

[1] This section had to be removed due to the non-disclosure agreement.

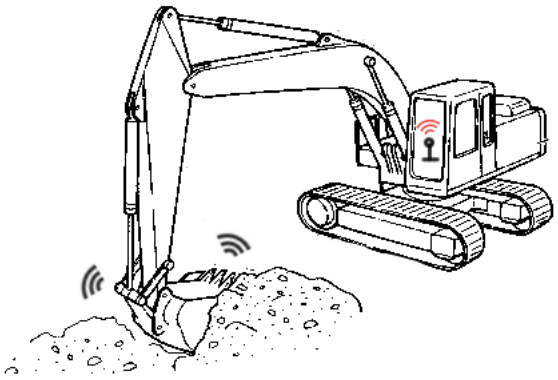

Figure 7.1: Excavator example

7.2 Control Methods

Besides the controllers that were evaluated in this thesis, two other control methods were planned but never tested. This was also due to the time limitation that arose because of changes in the hardware described in 7.3.2. These two controller method were the impedance controller and MPC. The impedance controller since it is one of the most used methods for haptic feedback [21] and MPC because of its constraint properties, it would be possible to prevent some angles or angular velocities by adding constraints. In addition to the controllers used, a scheduled LQR was tested for the control tasks instead of using the scheduled PID type of controllers. The controller was created to take care of all the tasks by scheduling the weights. This was never thoroughly tuned and did not reach a usable state. Even if the controller would be tuned for normal operation it would still suffer from the inaccuracy of the simulation of the mechanical stop. This could of course be solved by coupling the LQR with the event based controller, there was however insufficient time to fine tune two types of controllers for the regular tasks. The LQR has the possibility of working as good as the P, PD combination. As it was implemented the PD controller worked really well in order to follow the vehicle and resist sudden movement, with addition of the speed dependent P controller the steering of the vehicle felt smooth and realistic. The event based mechanical stop controller provided a sharp stop, it could however work better with a higher sampling frequency since the impulse is a high frequency response and would become smoother.

7.3 Issues

Like all projects, this thesis ran in to problems that had to be solved in one way or another, those were of modelling character as well as hardware character.

7.3.1 Angle of vehicle, γ

When modelling the vehicle an important issue arose, no explicit dynamic equation existed for γ. The equations were all dependent on γ and it was not possible to solve for γ to extract it, a possible solution would have been to measure rotations and angles on a real vehicle and establish a greybox model of the vehicle, there was however no time or possibility to perform such a test. The angle had to be estimated through double integration which affected the stability of the model. The authors tried to investigate previous work to find a solution to this, some works measured both rotating parts of the vehicle while others did not describe in detail how the model was constructed. This leads the authors to assume that the problem might have been part of their works as well.

7.3.2 Changes in hardware

The hardware design for this thesis changed drastically after about half time. Initially the project was meant to implement a electromagnet based haptic feedback, but due to a change of direction a DC motor solution was realised. Much of the theory and vehicle modelling could be salvage, but the hardware had to be completely rebuilt. This caused a major setback, since much of the scheduled time for this project was already spent. Because of this, the numbers of evaluated control methods and possible hardware solutions had to be simplified. For example, this is the reason why only PID and LQR are evaluated in this thesis. Some safety discussions were also planned, where the functional safety was to be a part of the thesis, this had to be cut out in order to manage the time limit of the project.

7.4 Future Work

The change in hardware direction caused some ideas to be unresolved. There were also some ideas discussed during this thesis how to extend the functionality of the hardware beyond the scope of this thesis. This section discusses some of these ideas.

7.4.1 Sensors

Angle

During testing of the potentiometer that was used to measure the angle of the joystick, it became apparent that it was temperature dependent. This was expected to some degree, but the amount exceeded the expectation. This was temporarily solved by calibrating the system each startup. But having to calibrate the system on each startup is not a preferred method. One way to potential solve this issue could be to change the polarity for one of the potentiometers, and use the ratio between the two. This could remove the temperature dependency and remove the need to calibrate the system.

Current

The relatively high level of noise from the current sensors resulted in some issues, since designing the filter became a trade-off between suppressing noise and delaying the signal. This could be investigated further, but a potential source for this noise could be the actual control signal itself, since the PWM is actually a square wave. Changing the motor controller could solve this, see section 7.4.2.

7.4.2 Motor Controller

Using a PWM signal to supply the DC motors can generate a high pitched sound if the frequency of the PWM signal is low enough for the human ear to hear. For a evaluation platform this is most likely not an issue, but it would not be a preferred choice for a commercial unit for haptic feedback. Using a DC supply instead of the PWM signal would remove this high pitched sound.

7.4.3 Gearbox

Gearboxes with multiple gearwheels were dismissed early in this projects, due to their relatively high friction. The friction in the gearboxes hindered the use of the joystick and some gearboxes also introduced a noticeable backlash. Another drawback was the mechanical sound produced by multiple gears. Alternative to mechanical gearboxes could be belts. For haptic feedback applications, belts might be preferred since those would have stepless transitions. This was never tested during this thesis, but could be interesting to investigate.

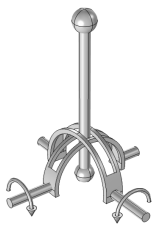

(a) Arcs above the pivot point

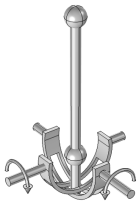

(b) Arcs below the pivot point

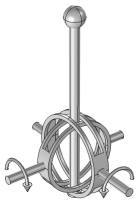

(c) Arcs around the pivot point

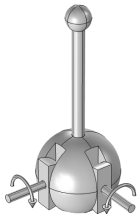

(d) Ball joint

Figure 7.2: Joysticks with two axis

Bibliography

[1] Mathworks simscape, http://se.mathworks.com/products/sl-design-optimization/, accessed: 2015-03-15.

[2] Arduino, http://www.arduino.cc, accessed: 2015-03-15.

[3] D. F. LeRoy, Steer-by-wire challenges hydraulics, Machine Design 78 (15) (2006) 52–55.
URL http://search.proquest.com/docview/217185426

[4] R. P. G. Collinson, S. A. (e-book collection), S. (e-book collection), Introduction to Avionics Systems, Springer US, Boston, MA, 2003.

[5] B. Hannaford, A. Okamura, Haptics, in: B. Siciliano, O. Khatib (Eds.), Springer Handbook of Robotics, Springer Berlin Heidelberg, 2008, pp. 719–739.
URL http://dx.doi.org/10.1007/978-3-540-30301-5_31

[6] Volvo Trucks dynamic steering, http://www.volvotrucks.com/trucks/uk-market/en-gb/trucks/volvo-fm/key-features/Pages/volvo-dynamic-steering.aspx, accessed: 2015-03-06.

[7] P. Nyman, K. Uhlén, Coordination of actuators for long heavy vehicle combinations using control allocation (2014).
URL http://studentarbeten.chalmers.se/publication/200460-coordination-of-actuators-for-long-heavy-vehicle-combinations-using-control-allocation

[8] M. Chen, Chieh. Tomizuka, Modeling and control of articulated vehicles (1997).
URL http://escholarship.org/uc/item/2k64h8k3

[9] J. B. Dragt, Modelling and control of an autonomous underground mine vehicle (2006).
URL http://hdl.handle.net/2263/27600

[10] K. Kuchenbecker, J. Fiene, G. Niemeyer, Improving contact realism through event-based haptic feedback, Visualization and Computer Graphics, IEEE Transactions on 12 (2) (2006) 219–230.

[11] J. S. PASCAL TRAVERSE, ISABELLE LACAZE, Airbus fly-by-wire: A process toward total dependability, 25TH INTERNATIONAL CONGRESS OF THE AERONAUTICAL SCIENCES.
URL http://www.icas.org/ICAS_ARCHIVE/ICAS2006/PAPERS/050.PDF

[12] C. FAVRE, Fly-by-wire for commercial aircraft: the airbus experience, International Journal of Control.
URL http://www.tandfonline.com/doi/pdf/10.1080/00207179408923072

[13] J. J. Gil, I. Díaz, P. Ciáurriz, M. Echeverría, New driving control system with haptic feedback: Design and preliminary validation tests, Transportation Research Part C: Emerging Technologies 33 (0) (2013) 22 – 36.
URL http://www.sciencedirect.com/science/article/pii/S0968090X13000776

[14] J. J. Gil, I. Diaz, X. Justo, P. Ciaurriz, Educational haptic controller based on arduino platform, IEEE, 2014, pp. 1–7.
URL http://ieeexplore.ieee.org/xpl/articleDetails.jsp?arnumber=6900140

[15] D. Schramm, M. Hiller, R. Bardini, Equations of Motion of Complex Multibody Systems, Springer Berlin Heidelberg, 2014.
URL http://dx.doi.org/10.1007/978-3-540-36045-2_4

[16] K. J. Åström, R. M. Murray, Feedback systems: an introduction for scientists and engineers, Princeton University Press, Princeton, N.J, 2008.

[17] MATLAB Simulink pid controller tuning in simulink, http://se.mathworks.com/help/slcontrol/gs/automated-tuning-of-simulink-pid-controller-block.html, accessed: 2015-03-08.

[18] Velleman motor shield, http://www.vellemanusa.com/downloads/0/modules/usermanual_vma03.pdf, accessed: 2015-03-15.

[19] R. Lilja, A localisation and navigation system for an autonomous wheel loader, accessed: 2015-03-10 (2011).
URL http://www.idt.mdh.se/utbildning/exjobb/files/TR1095.pdf

[20] Q. He, X. Fan, D. Ma, Full bicycle dynamic model for interactive bicycle simulator, Journal of Computing and Information Science in Engineering 5 (4) (2005) 373.
URL www.summon.com

[21] O. M. E. M. C. J. El Saddik, A., Haptics Technologies: Bringing Touch to Multimedia, Springer-Verlag Berlin Heidelberg, University of Ottawa, 2011.

[22] J. Brody, P. Yager, R. Goldstein, R. Austin, Biotechnology at low Reynolds numbers, Biophysical Journal 71 (6) (1996) 3430–3441.
URL `http://linkinghub.elsevier.com/retrieve/pii/S0006349596795383`

A

Datasheet: DC Motor

RS-555SH

★输出：0.7W-40W（大约）
★重量：55g（大约）

典型应用领域：
家用电器

★OUTPUT:0.7W-40W (APPROX)
★WEIGHT:55g (APPROX)

Typical Applications:
Home Appliances

■性能参数 Performance Parameters

型号 Model		电压 Voltage		无负载 No Load		在最大效率时 At Maximum Efficiency					堵转 Stall		
		工作范围 Operating Range	额定 Nominal	速度 Speed	电流 Current	速度 Speed	电流 Current	扭矩 Torque		输出 Output	扭矩 Torque		电流 Current
		V	V	r/min	A	r/min	A	mN·m	g·cm	W	mN·m	g·cm	A
RS-555SH	15260	12~28	24	1850	0.026	1560	0.15	14.70	150	2.4	84.529	862.54	0.72

■机械尺寸 Mechanical Dimensions:mm

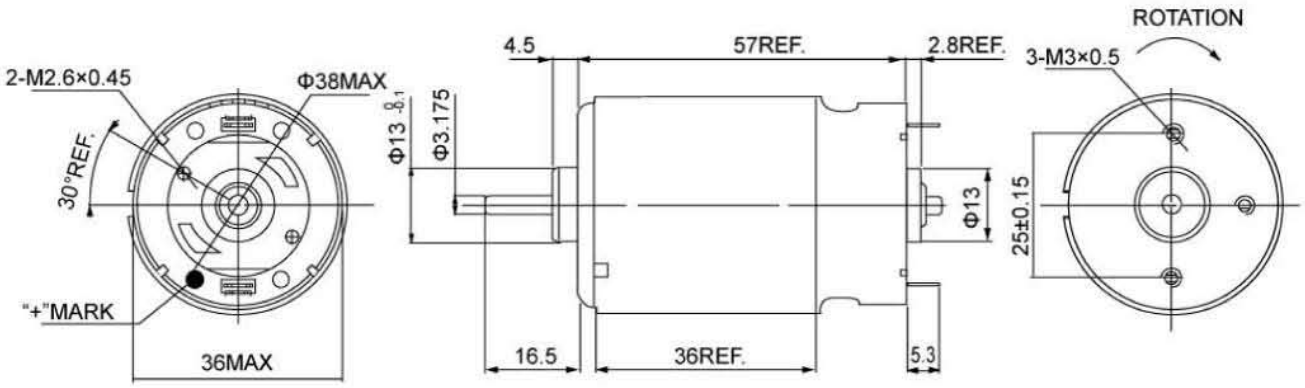

■电机特性曲线 Motor Performance Curves

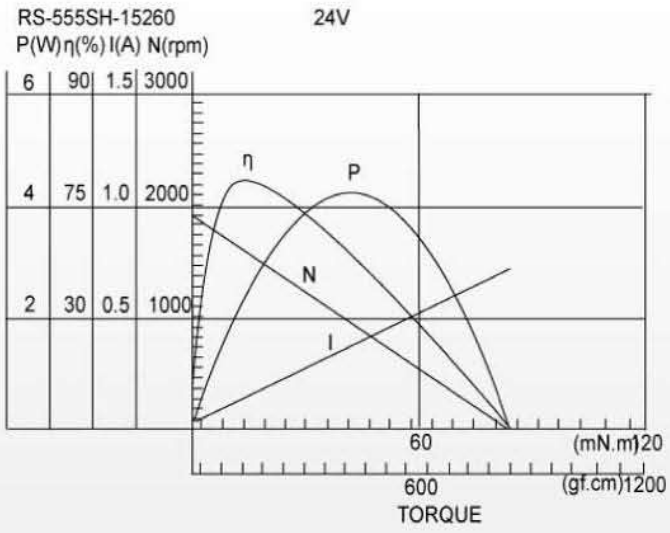

B

Datasheet: Potentiometer

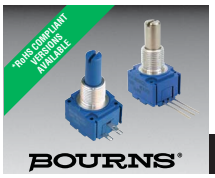

Features

- Available in a variety of pin-out configurations
- Virtually infinite electrical circuit isolation
- Model 96 sealed for board wash
- Metal or plastic shaft options

BOURNS® PRO AUDIO

Additional Features

- DPST and DPDT switch options
- RoHS compliant versions available*

91, 92, 93, 94, 95, 96 - 5/8 " Square Single-Turn Panel Control
97, 99 - 5/8 " Square Single-Turn Panel Control with Rotary Switch

BOURNS®

Potentiometer Specifications

Initial Electrical Characteristics[1]	Conductive Plastic Element	Cermet Element
Standard Resistance Range		
Linear Tapers (A, B, E, & H)	(B & E) 1 K ohms to 1 megohm	(A & H) 100 ohms to 1 megohm
Audio Tapers (C, D, F, G, S, & T)	(D,G,S, & T) 1 K ohms to 1 megohm	(C & F) 1 K ohms to 1 megohm
Total Resistance Tolerance	10 % or 20 %	5% or 10%
Independent Linearity	±5 %	±5 %
Absolute Minimum Resistance	2 ohms maximum	2 ohms maximum
Effective Electrical Angle	(Linear tapers) 240 ° ± 5 °	(Linear tapers) 240 ° ± 6 °
	(Audio tapers) 225 ° ± 5 °	(Audio tapers) 225 ° ± 6 °
Contact Resistance Variation	±1 %	±1 % or 3 ohms (whichever is greater)
Dielectric Withstanding Voltage (MIL-STD-202, Method 301)		
Sea Level	1,500 VAC minimum	1,500 VAC minimum
70,000 Feet	500 VAC minimum	500 VAC minimum
Insulation Resistance (500 VDC)	1,000 megohms minimum	1,000 megohms minimum
Power Rating (Voltage Limited By Power Dissipation or 350 VAC, Whichever Is Less)		
+70 °C Single Section Assembly	(Linear tapers) 0.5 watt	(Linear tapers) 2 watts
	(Audio tapers) 0.25 watt	(Audio tapers) 1 watt
+70 °C Multiple Section Assembly	(Linear tapers) 0.5 watt/section	(Linear tapers) 1 watt/section
	(Audio tapers) 0.25 watt/section	(Audio tapers) 0.5 watt/section
+125 °C	0 watt	0 watt
Theoretical Resolution	Essentially infinite	Essentially infinite

Environmental Characteristics[1]

Operating Temperature Range	-40 °C to +125 °C	-40 °C to +125 °C
Storage Temperature Range	-55 °C to +125 °C	-55 °C to +125 °C
Temperature Coefficient Over Storage Temperature Range	±1,000 ppm/°C	±150 ppm/°C
Vibration (Single Section)	15 G	15 G
Total Resistance Shift	±2 % maximum	±2 % maximum
Voltage Ratio Shift	±5 % maximum	±5 % maximum
Shock (Single Section)	30 G	30 G
Total Resistance Shift	±2 % maximum	±2 % maximum
Voltage Ratio Shift	±5 % maximum	±5 % maximum
Load Life	1,000 hours	1,000 hours
Total Resistance Shift	±10 % maximum	±5 % maximum
Rotational Life (No Load)	100,000 cycles	100,000 cycles
Total Resistance Shift	(Linear tapers) 10 ohms or ±15 % TRS max. (whichever is greater)	(All tapers) ±5 % TRS max.
	(Audio tapers) ±20 % maximum	
Contact Resistance Variation @ 50,000 cycles	(Linear tapers) ±2 %	±2 %
	(Audio tapers) ±3 %	±3 %
Moisture Resistance (MIL-STD-202, Method 103, Condition B)		
Total Resistance Shift	(Linear tapers) ±10 % TRS maximum	(All tapers) ±5 % TRS maximum
	(Audio tapers) ±20 % TRS maximum	
Insulation Resistance (500 VDC)	100 megohms minimum	100 megohms minimum
IP Rating (Model 96)	IP 65	IP 65
(All Others)	IP 40	IP 40

*RoHS Directive 2002/95/EC Jan 27 2003 including Annex
Specifications are subject to change without notice.
Customers should verify actual device performance in their specific applications.

91, 92, 93, 94, 95, 96 - 5/8 " Square Single-Turn Panel Control
97, 99 - 5/8 " Square Single-Turn Panel Control with Rotary Switch

BOURNS®

Potentiometer Specifications

Mechanical Characteristics[1]

Stop Strength (1/4 " D shaft)	45.19 N-cm (4 lb.-in.)
(1/8 " D shaft)	33.89 N-cm (3 lb.-in.)
Mechanical Angle	300 ° ±5 °
Torque	
Starting	0.3 max. above average running torque
Running Torque	
Single or Dual Section (A ,D & R Bushings)	0.21 to 1.06 N-cm (0.3 to 1.5 oz.-in.)
Single or Dual Section (C & U Bushings)	0.14 to 1.06 N-cm (0.2 to 1.5 oz.-in.)
Mounting	(Metal Bushing) 1.7-2.0 N-m (15-18 lb.-in.) maximum
	Plastic Bushing) 56-79 N-cm (5-7 lb.-in.) maximum
Variation	0.35 N-cm (0.5 oz.-in.) maximum in 45 ° shaft travel
Weight (Single Section, Plastic Bushing)	7.3 grams nominal
Weight (Single Section, Metal Bushing)	12.7 grams nominal
(Each Additional Section)	4 grams nominal
Terminals	Printed circuit terminals, J-Hooks or solder lugs
Soldering Condition	Recommended hand soldering using Sn95/Ag5 no clean solder, 0.025 " wire diameter. Maximum temperature 399 °C (750 °F) for 3 seconds. No wash process to be used with no clean flux.
Marking	Manufacturer's trademark, date code, resistance, manufacturer's part number
Ganging (Multiple Section Potentiometers)	2 cups maximum
Hardware	One lockwasher and one mounting nut is shipped with each potentiometer, except where noted in the part number.

NOTE: All Model 90 performance specifications do not apply to units subjected to printed circuit board cleaning procedures, except for the sealed version (Model 96).

[1]At room ambient: +25 °C nominal and 50 % relative humidity nominal, except as noted.

Specifications are subject to change without notice.
Customers should verify actual device performance in their specific applications.

91, 92, 93, 94, 95, 96 - 5/8 " Square Single-Turn Panel Control
97, 99 - 5/8 " Square Single-Turn Panel Control with Rotary Switch

BOURNS®

Rotary Switch Specifications

Initial Electrical Characteristics[1]

Contacts:	
DPST	N.O/N.O., N.C./N.C. or N.O./N.C.
DPDT	2 N.O./N.C. (break before make)
Power Rating (Resistive Load):	
DPST	2 A @ 125 volts RMS-60 Hz or 2 A @ 28 VDC, 1 A @ 250 volts RMS-60 Hz
DPDT	1 A @ 125 volts RMS-60 Hz or 1 A @ 28 VDC
Contact Resistance (0.1 VDC-10 mA)	10 milliohms nominal
Contact Bounce	5 milliseconds maximum
Dielectric Withstanding Voltage (MIL-STD-202, Method 301)	
Sea Level	1500 VAC minimum
Insulation Resistance	1000 megohms minimum

Environmental Characteristics[1]

Operating Temperature Range	0 °C to +70 °C
Exposure Temperature Range	-65 °C to +125 °C
Vibration (Dual Section)	8 G
Contact Resistance	10 milliohms maximum
Contact Bounce	0.1 millisecond maximum
Shock (Dual Section)	20 G
Contact Resistance	10 milliohms maximum
Contact Bounce	0.1 millisecond maximum
Rotational Life	25,000 cycles
Switch Actuating Torque (50% Duty cycle @ Rated Power Load)	1.41 to 4.94 N-cm (2 to 7 oz.-in.)
Contact Resistance	100 milliohms maximum
Moisture Resistance (MIL-STD-202, Method 106, Condition B)	
Contact Resistance (0.1 VDC-10 mA)	10 milliohms maximum
Insulation Resistance (After 24 Hours @ Room Temperature) (500 VDC)	100 megohms minimum
Housing Material	High temperature, flame retardant, thermosetting plastic

Mechanical Characteristics[1]

Actuating Torque (Each Section, Switch Module Only)	3.53 to 10.59 N-cm (5 to 15 oz.-in.)
Running Torque (Out of Detent, 2-4 Module Assembly)	0.21 to 1.41 N-cm (0.3 to 2 oz.-in.)
Detent	CW or CCW standard
Actuation Angle	20 ° ±5 °
Contact Materials	Fine silver with gold overlay
Terminal Styles	Solder lug only
Standard Orientation	In-line with control terminals
Optional	Rotated 90 ° CCW from standard
Terminal Strength (Before and After Soldering Heat Exposure)	0.9 kg (2 lbs.) minimum

NOTE: Model 99 performance specifications do not apply to units subjected to printed circuit board cleaning procedures.

[1]At room ambient: +25 °C nominal and 50 % relative humidity nominal, except as noted.

Specifications are subject to change without notice.
Customers should verify actual device performance in their specific applications.

91, 92, 93, 94, 95, 96, 97, 99 - 5/8 " Square Single-Turn

BOURNS®

Product Dimensions

Model 91 & 96 PC Pin Terminals, In-Line

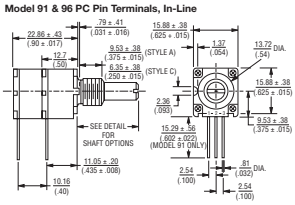

Model 92 J-Hooked Terminals, In-Line

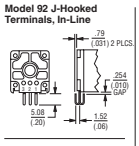

Model 94 J-Hooked Terminals, "L" Pattern

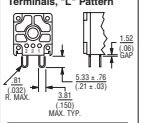

Bushing Styles

3/8 THREADLESS (9.53 mm) (STYLE "D")
3/8-32 UNEF (9.53 mm) (STYLE "A")
1/4-32 UNEF (6.35 mm) (STYLE "C")
M10 X 0.75-6g (STYLE "F")
M7 X 0.75-6g (STYLE "U")

Model 93 PC Pin Terminals, "L" Pattern

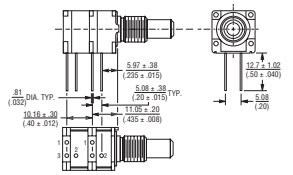

Model 95 Solder Lug Terminals, "Triangular" Pattern

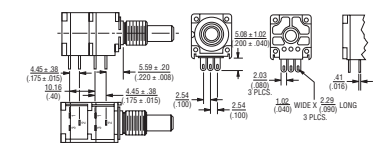

TOLERANCES EXCEPT AS SHOWN: DECIMAL .XXX ± .128 (.015) FRACTION ± 1/64 .XX ± .005 (.38) ANGLE ±5 °

DIMENSIONS: MM (INCHES)

Model 97 1st Cup Same As Model 93 (2nd Cup - Switch)

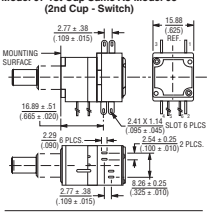

Model 99 1st Cup Same As Model 95 (2nd Cup - Switch)

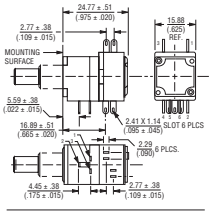

Switch Module Variations Shaft Flat Orientation

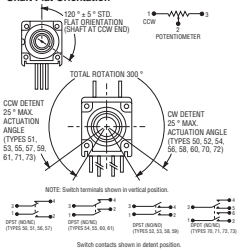

Specifications are subject to change without notice.
Customers should verify actual device performance in their specific applications.

91, 92, 93, 94, 95, 96, 97, 99 - 5/8 " Square Single-Turn

BOURNS®

Product Dimensions

Plastic Shaft Styles

SHAFT TYPE "B" (USES BUSHING A OR D)

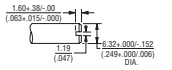

STD. LENGTHS:

12.70 (.500)	15.88 (.625)	19.05 (.750)	22.23 (.875)

SHAFT TYPE "D" (USES BUSHING C)

STD. LENGTHS:

12.70 (.500)	15.88 (.625)	19.05 (.750)

SHAFT TYPE "T" (USES BUSHING U)

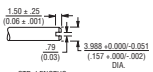

STD. LENGTHS:

12.00 (.472)	16.00 (.630)	22.00 (.866)

SHAFT TYPE "C" (USES BUSHING A OR D)

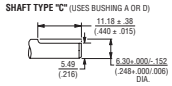

STD. LENGTHS:

22.23 (.875)

SHAFT TYPE "R" (USES BUSHING R)

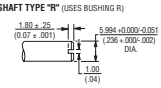

STD. LENGTHS:

16.0 (.630)	19.0 (.748)	22.0 (.866)

SHAFT TYPE "W" (USES BUSHING A OR D)

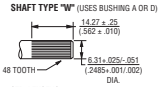

STD. LENGTHS:

25.40 (1.00)

Metal Shaft Styles

SHAFT TYPE "A" (USES BUSHING A)

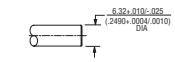

STD. LENGTHS:

12.70 (.500)	15.88 (.625)	19.05 (.750)	22.23 (.875)	25.4 (1.000)

SHAFT TYPE "H" (USES BUSHING A)

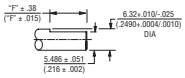

STD. LENGTHS:

12.70 (.500)	15.88 (.625)	19.05 (.750)	22.23 (.875)	25.4 (1.000)

FLAT LENGTH "F":

1.60 (.063)	4.78 (.188)	7.95 (.313)	11.13 (.438)	14.30 (.563)

SHAFT TYPE "V" (USES BUSHING U)

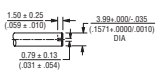

STD. LENGTHS:

12.0 (.472)	16.0 (.630)	19.0 (.748)	22.0 (.866)

SHAFT TYPE "G" (USES BUSHING A)

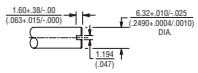

STD. LENGTHS:

12.70 (.500)	15.88 (.625)	19.05 (.750)	22.23 (.875)	25.4 (1.000)

SHAFT TYPE "J" (USES BUSHING R)

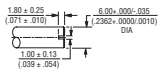

STD. LENGTHS:

12.0 (.472)	16.0 (.630)	19.0 (.748)	22.0 (.866)

SHAFT TYPE "Y" (USES BUSHING A)

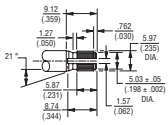

STD. LENGTHS:

19.05 (.750)

DIMENSIONS: MM / (INCHES)

TOLERANCES EXCEPT AS SHOWN: .XX = ± .02 (.050); .XXX = ± .005 (.127); .XXXX = ± .0005 (.0127)

Specifications are subject to change without notice.
Customers should verify actual device performance in their specific applications.

How to Order 90 Series Panel Controls

BOURNS®

91	A	2	A	-	A	28	-	A	15	/	A15	L	Models 91 - 96: Part number for multiple section potentiometers must have a taper and resistance value for each section.
99	A	2	A	-	B	28	-	A	15	/	R51	L	Models 97 & 99: Part number must contain a switch type.

ANTI-ROTATION LUG	
A	**Single .305 " (7.8 mm) R, 90 °CW**
C	Single .305 " (7.8 mm) R, 270 °CW
D	**No Lug**

# SECTIONS		APPLICABLE MODELS
1	**Single**	**Models 91 Thru 96 Only**
2	Dual	All Models, 2nd Section is a Switch in Model 99

BUSHING	
A	**Metal Plain 3/8 " (9.53 mm) D x 3/8 " (9.53 mm) L**
C	**Metal Plain 1/4 " (6.35 mm) D x 1/4 " (6.35 mm) L**
D	Plastic Unthreaded 3/8 " (9.53 mm) D x 3/8 " (9.53 mm) L
R	**Metal Plain 10 mm D x 9 mm L**
U	**Metal Plain 7 mm D x 9 mm L**

SHAFT LENGTH (FMS)		AVAILABLE ONLY IN BUSHING
Code	Description	Code
16	1/2 "L	A, C, D
20	5/8 "L	A, C, D
24	**3/4 "L**	A, C, D
28	**7/8 "L**	**A, D**
32	1 "L	A, D
METRIC		
12	12 mmL	U
16	16 mmL	R, U
19	19 mmL	R
22	**22 mmL**	R, U

RoHS IDENTIFIER	
L	**Compliant**
Blank	**Non-Compliant**

SWITCH TYPE (MODELS 97 & 99 ONLY)
(R50) DPST N.O./N.C. CW Detent In-Line Term
(R51) DPST N.O./N.C. CCW Detent In-Line Term
(R52) DPST N.O./N.O. CW Detent In-Line Term
(R53) DPST N.O./N.O. CCW Detent In-Line Term
(R54) DPST N.C./N.C. CW Detent In-Line Term
(R55) DPST N.C./N.C. CCW Detent In-Line Term
(R56) DPST N.O./N.C. CW Detent Horz Term
(R57) DPST N.O./N.C. CCW Detent Horz Term
(R58) DPST N.O./N.O. CW Detent Horz Term
(R59) DPST N.O./N.O. CCW Detent Horz Term
(R60) DPST N.C./N.C. CW Detent Horz Term
(R61) DPST N.C./N.C. CCW Detent Horz Term
(R70) DPDT CW Detent In-Line Term
(R71) DPDT CCW Detent In-Line Term
(R72) DPDT CW Detent Horz Term
(R73) DPDT CCW Detent Horz Term

MODEL	
91	**Single-Turn, In-Line PC Pins**
92	Single-Turn, In-Line J-Hooks
93	Single-Turn, L-Pattern PC Pins
94	Single-Turn, L-Pattern J-Hooks
95	Single-Turn, Triangle-Pattern Solder Lugs
96	Single-Turn, In-Line PC Pins, Sealed*
97	Single-Turn, L-Pattern PC Pins w/Switch
99	**Single-Turn, Triangle-Pattern Solder Lugs w/Switch**

*Model 96 is not available in multi-gang versions.

SHAFT TYPE		AVAILABLE ONLY IN LENGTHS (CODE)	AVAILABLE ONLY IN BUSHINGS (CODE)
B	**Plastic Single Slotted 1/4 " (6.35 mm) D**	16,20,24,28	**A,D**
C	**Plastic Single Flatted 1/4" (6.35 mm) D**	24,28	**A,D**
D	Plastic Single Plain 1/8" (3.18 mm) D	16,20,24	C
R	**Plastic Single Slotted 6 mm D**	Metric 16,19,22	R
T	**Plastic Single Slotted 4 mm D**	Metric 16,19,22	U
W	Plastic Single Knurled 1/4" (6.35 mm) D	32	**A,D**
A	**Metal Single Plain 1/4" (6.35 mm) D**	16,20,24,28,32	**A**
G	**Metal Single Slotted 1/4" (6.35 mm) D**	16,20,24,28,32	**A**
H	**Metal Single Flatted 1/4" (6.35 mm) D**	16,20,24,28,32	**A**
J	**Metal Single Slotted 6 mm D**	Metric 12,16,19,22	R
V	**Metal Single Slotted 4 mm D**	Metric 12,16,19,22	U
Y	**Metal Single Knurled 1/4" (6.35 mm) D**	24	**A**

ELEMENT TAPER TYPE/TOLERANCE		RESISTANCE CODE VALUE IN OHMS	
(A)	**Linear Cermet ±10 %**	(05) - 100	(30) - 15 K
(H)	Linear Cermet ±5 %	(28) - 150	(16) - 20 K
		(06) - 200	(17) - 25 K
		(07) - 250	**(18) - 50 K**
		(08) - 500	(19) - 75 K
		(09) - 750	**(20) - 100 K**
		(10) - 1 K	(31) - 150 K
		(29) - 1.5 K	(21) - 200 K
		(11) - 2 K	(22) - 250 K
		(12) - 2.5 K	(23) - 500 K
		(13) - 5 K	(24) - 750 K
		(14) - 7.5 K	(25) - 1 M
		(15) - 10 K	
(B)	**Linear C-P ±20 %**	**(10) - 1 K**	**(18) - 50 K**
(E)	Linear C-P ±10 %	(12) - 2.5 K	**(20) - 100 K**
		(13) - 5 K	(22) - 250 K
		(15) - 10 K	(23) - 500 K
		(16) - 20 K	(25) - 1 M
		(17) - 25 K	
(C)	CW Audio Cermet ±10 %	(10) - 1 K	(18) - 50 K
(D)	CW Audio C-P ±20 %	(12) - 2.5 K	(20) - 100 K
(F)	CCW Audio Cermet ±10 %	(13) - 5 K	(22) - 250 K
(G)	CCW Audio C-P ±20 %	(15) - 10 K	(23) - 500 K
(S)	CW Audio C-P ±10 %	(17) - 25 K	(25) - 1 M
(T)	CCW Audio C-P ± 10 %		

Boldface features are Bourns standard options. All others are available with higher minimum order quantities.

REV. 02/10

Specifications are subject to change without notice.
Customers should verify actual device performance in their specific applications.

C

Datasheet: Current Sensor

Fully Integrated, Hall Effect-Based Linear Current Sensor with 2.1 kVRMS Voltage Isolation and a Low-Resistance Current Conductor

Features and Benefits

- Low-noise analog signal path
- Device bandwidth is set via the new FILTER pin
- 5 µs output rise time in response to step input current
- 50 kHz bandwidth
- Total output error 1.5% at T_A = 25°C, and 4% at –40°C to 85°C
- Small footprint, low-profile SOIC8 package
- 1.2 mΩ internal conductor resistance
- 2.1 kV_{RMS} minimum isolation voltage from pins 1-4 to pins 5-8
- 5.0 V, single supply operation
- 66 to 185 mV/A output sensitivity
- Output voltage proportional to AC or DC currents
- Factory-trimmed for accuracy
- Extremely stable output offset voltage
- Nearly zero magnetic hysteresis
- Ratiometric output from supply voltage

Package: 8 pin SOIC (suffix LC)

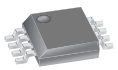

Approximate Scale 1:1

Description

The Allegro® ACS712 provides economical and precise solutions for AC or DC current sensing in industrial, automotive, commercial, and communications systems. The device package allows for easy implementation by the customer. Typical applications include motor control, load detection and management, switched-mode power supplies, and overcurrent fault protection.

The device consists of a precise, low-offset, linear Hall sensor circuit with a copper conduction path located near the surface of the die. Applied current flowing through this copper conduction path generates a magnetic field which is sensed by the integrated Hall IC and converted into a proportional voltage. Device accuracy is optimized through the close proximity of the magnetic signal to the Hall transducer. A precise, proportional voltage is provided by the low-offset, chopper-stabilized BiCMOS Hall IC, which is programmed for accuracy after packaging.

The output of the device has a positive slope (>$V_{IOUT(Q)}$) when an increasing current flows through the primary copper conduction path (from pins 1 and 2, to pins 3 and 4), which is the path used for current sensing. The internal resistance of this conductive path is 1.2 mΩ typical, providing low power

Continued on the next page…

Typical Application

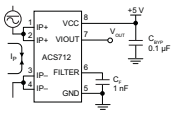

Application 1. The ACS712 outputs an analog signal, V_{OUT}, that varies linearly with the uni- or bi-directional AC or DC primary sensed current, I_P, within the range specified. C_F is recommended for noise management, with values that depend on the application.

Description (continued)

loss. The thickness of the copper conductor allows survival of the device at up to 5× overcurrent conditions. The terminals of the conductive path are electrically isolated from the sensor leads (pins 5 through 8). This allows the ACS712 current sensor to be used in applications requiring electrical isolation without the use of opto-isolators or other costly isolation techniques.

The ACS712 is provided in a small, surface mount SOIC8 package. The leadframe is plated with 100% matte tin, which is compatible with standard lead (Pb) free printed circuit board assembly processes. Internally, the device is Pb-free, except for flip-chip high-temperature Pb-based solder balls, currently exempt from RoHS. The device is fully calibrated prior to shipment from the factory.

Selection Guide

Part Number	Packing*	T_{OP} (°C)	Optimized Range, I_P (A)	Sensitivity, Sens (Typ) (mV/A)
ACS712ELCTR-05B-T	Tape and reel, 3000 pieces/reel	–40 to 85	±5	185
ACS712ELCTR-20A-T	Tape and reel, 3000 pieces/reel	–40 to 85	±20	100
ACS712ELCTR-30A-T	Tape and reel, 3000 pieces/reel	–40 to 85	±30	66

*Contact Allegro for additional packing options.

Absolute Maximum Ratings

Characteristic	Symbol	Notes	Rating	Units
Supply Voltage	V_{CC}		8	V
Reverse Supply Voltage	V_{RCC}		–0.1	V
Output Voltage	V_{IOUT}		8	V
Reverse Output Voltage	V_{RIOUT}		–0.1	V
Output Current Source	$I_{IOUT(Source)}$		3	mA
Output Current Sink	$I_{IOUT(Sink)}$		10	mA
Overcurrent Transient Tolerance	I_P	100 total pulses, 250 ms duration each, applied at a rate of 1 pulse every 100 seconds.	60	A
Maximum Transient Sensed Current	I_R(max)	Junction Temperature, $T_J < T_J$(max)	60	A
Nominal Operating Ambient Temperature	T_A	Range E	–40 to 85	°C
Maximum Junction	T_J(max)		165	°C
Storage Temperature	T_{stg}		–65 to 170	°C

TÜV America
Certificate Number:
U8V 06 05 54214 010

Parameter	Specification
Fire and Electric Shock	CAN/CSA-C22.2 No. 60950-1-03 UL 60950-1:2003 EN 60950-1:2001

Allegro MicroSystems, Inc.
115 Northeast Cutoff, Box 15036
Worcester, Massachusetts 01615-0036 (508) 853-5000
www.allegromicro.com

Functional Block Diagram

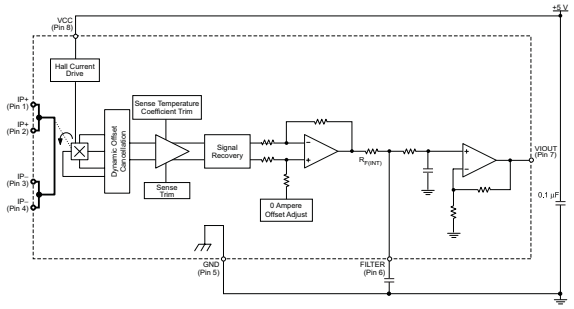

Pin-out Diagram

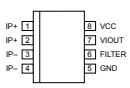

Terminal List Table

Number	Name	Description
1 and 2	IP+	Terminals for current being sensed; fused internally
3 and 4	IP–	Terminals for current being sensed; fused internally
5	GND	Signal ground terminal
6	FILTER	Terminal for external capacitor that sets bandwidth
7	VIOUT	Analog output signal
8	VCC	Device power supply terminal

Allegro MicroSystems, Inc.
115 Northeast Cutoff, Box 15036
Worcester, Massachusetts 01615-0036 (508) 853-5000
www.allegromicro.com

COMMON OPERATING CHARACTERISTICS[1] over full range of T_{OP}, C_F = 1 nF, and V_{CC} = 5 V, unless otherwise specified

Characteristic	Symbol	Test Conditions	Min.	Typ.	Max.	Units
ELECTRICAL CHARACTERISTICS						
Supply Voltage	V_{CC}		4.5	5.0	5.5	V
Supply Current	I_{CC}	V_{CC} = 5.0 V, output open	6	8	11	mA
Output Zener Clamp Voltage	V_Z	I_{CC} = 11 mA, T_A = 25°C	6	8.3	–	V
Output Resistance	R_{IOUT}	I_{IOUT} = 1.2 mA, T_A=25°C	–	1	2	Ω
Output Capacitance Load	C_{LOAD}	VIOUT to GND	–	–	10	nF
Output Resistive Load	R_{LOAD}	VIOUT to GND	4.7	–	–	kΩ
Primary Conductor Resistance	$R_{PRIMARY}$	T_A = 25°C	–	1.2	–	mΩ
RMS Isolation Voltage	V_{ISORMS}	Pins 1-4 and 5-8; 60 Hz, 1 minute, T_A=25°C	2100	–	–	V
DC Isolation Voltage	V_{ISODC}	Pins 1-4 and 5-8; 1 minute, T_A=25°C	–	5000	–	V
Propagation Time	t_{PROP}	$I_P = I_P$(max), T_A = 25°C, C_{OUT} = open	–	3	–	µs
Response Time	$t_{RESPONSE}$	$I_P = I_P$(max), T_A = 25°C, C_{OUT} = open	–	7	–	µs
Rise Time	t_r	$I_P = I_P$(max), T_A = 25°C, C_{OUT} = open	–	5	–	µs
Frequency Bandwidth	f	–3 dB, T_A = 25°C; I_P is 10 A peak-to-peak	50	–	–	kHz
Nonlinearity	E_{LIN}	Over full range of I_P	–	±1	±1.5	%
Symmetry	E_{SYM}	Over full range of I_P	98	100	102	%
Zero Current Output Voltage	$V_{IOUT(Q)}$	Bidirectional; I_P = 0 A, T_A = 25°C	–	V_{CC} × 0.5	–	V
Magnetic Offset Error	V_{ERROM}	I_P = 0 A, after excursion of 5 A	–	0	–	mV
Clamping Voltage	V_{CH}		Typ. –110	V_{CC} × 0.9375	Typ. +110	mV
	V_{CL}		Typ. –110	V_{CC} × 0.0625	Typ. +110	mV
Power-On Time	t_{PO}	Output reaches 90% of steady-state level, T_J = 25°C, 20 A present on leadframe	–	35	–	µs
Magnetic Coupling[2]			–	12	–	G/A
Internal Filter Resistance[3]	$R_{F(INT)}$			1.7		kΩ

[1]Device may be operated at higher primary current levels, I_P, and ambient, T_A, and internal leadframe temperatures, T_{OP}, provided that the Maximum Junction Temperature, T_J(max), is not exceeded.
[2]1G = 0.1 mT.
[3]$R_{F(INT)}$ forms an RC circuit via the FILTER pin.

COMMON THERMAL CHARACTERISTICS[1]

			Min.	Typ.	Max.	Units
Operating Internal Leadframe Temperature	T_{OP}	E range	–40	–	85	°C
					Value	Units
Junction-to-Lead Thermal Resistance[2]	$R_{\theta JL}$	Mounted on the Allegro ASEK 712 evaluation board			5	°C/W
Junction-to-Ambient Thermal Resistance	$R_{\theta JA}$	Mounted on the Allegro 85-0322 evaluation board, includes the power consumed by the board			23	°C/W

[1]Additional thermal information is available on the Allegro website.
[2]The Allegro evaluation board has 1500 mm² of 2 oz. copper on each side, connected to pins 1 and 2, and to pins 3 and 4, with thermal vias connecting the layers. Performance values include the power consumed by the PCB. Further details on the board are available from the Frequently Asked Questions document on our website. Further information about board design and thermal performance also can be found in the Applications Information section of this datasheet.

Allegro MicroSystems, Inc.
115 Northeast Cutoff, Box 15036
Worcester, Massachusetts 01615-0036 (508) 853-5000
www.allegromicro.com

x05A PERFORMANCE CHARACTERISTICS T_{OP} = –40°C to 85°C[1], C_F = 1 nF, and V_{CC} = 5 V, unless otherwise specified

Characteristic	Symbol	Test Conditions	Min.	Typ.	Max.	Units
Optimized Accuracy Range	I_P		–5	–	5	A
Sensitivity[2]	$Sens_{TA}$	Over full range of I_P, T_A = 25°C	–	185	–	mV/A
	$Sens_{TOP}$	Over full range of I_P	178	–	193	mV/A
Noise	$V_{NOISE(PP)}$	Peak-to-peak, T_A= 25°C, 185 mV/A programmed Sensitivity, C_F=4.7 nF, C_{OUT} = open, 20 kHz bandwidth	–	45	–	mV
		Peak-to-peak, T_A = 25°C, 185 mV/A programmed Sensitivity, C_F = 47 nF, C_{OUT} = open, 2 kHz bandwidth	–	20	–	mV
		Peak-to-peak, T_A = 25°C, 185 mV/A programmed Sensitivity, C_F = 1 nF, C_{OUT} = open, 50 kHz bandwidth	–	75	–	mV
Electrical Offset Voltage	V_{OE}	I_P = 0 A	–40	–	40	mV
Total Output Error[3]	E_{TOT}	I_P =±5 A, T_A = 25°C	–	±1.5	–	%

[1]Device may be operated at higher primary current levels, I_P, and ambient temperatures, T_{OP}, provided that the Maximum Junction Temperature, T_J(max), is not exceeded.
[2]At –40°C Sensitivity may shift as much 9% outside of the datasheet limits.
[3]Percentage of I_P, with I_P = 5 A. Output filtered.

x20A PERFORMANCE CHARACTERISTICS T_{OP} = –40°C to 85°C[1], C_F = 1 nF, and V_{CC} = 5 V, unless otherwise specified

Characteristic	Symbol	Test Conditions	Min.	Typ.	Max.	Units
Optimized Accuracy Range	I_P		–20	–	20	A
Sensitivity[2]	$Sens_{TA}$	Over full range of I_P, T_A = 25°C	–	100	–	mV/A
	$Sens_{TOP}$	Over full range of I_P	97	–	103	mV/A
Noise	$V_{NOISE(PP)}$	Peak-to-peak, T_A= 25°C, 100 mV/A programmed Sensitivity, C_F=4.7 nF, C_{OUT} = open, 20 kHz bandwidth	–	24	–	mV
		Peak-to-peak, T_A = 25°C, 100 mV/A programmed Sensitivity, C_F = 47 nF, C_{OUT} = open, 2 kHz bandwidth	–	10	–	mV
		Peak-to-peak, T_A = 25°C, 100 mV/A programmed Sensitivity, C_F = 1 nF, C_{OUT} = open, 50 kHz bandwidth	–	40	–	mV
Electrical Offset Voltage	V_{OE}	I_P = 0 A	–30	–	30	mV
Total Output Error[3]	E_{TOT}	I_P =±20 A, T_A = 25°C	–	±1.5	–	%

[1]Device may be operated at higher primary current levels, I_P, and ambient temperatures, T_{OP}, provided that the Maximum Junction Temperature, T_J(max), is not exceeded.
[2]At –40°C Sensitivity may shift as much 9% outside of the datasheet limits.
[3]Percentage of I_P, with I_P = 20 A. Output filtered.

x30A PERFORMANCE CHARACTERISTICS T_{OP} = –40°C to 85°C[1], C_F = 1 nF, and V_{CC} = 5 V, unless otherwise specified

Characteristic	Symbol	Test Conditions	Min.	Typ.	Max.	Units
Optimized Accuracy Range	I_P		–30	–	30	A
Sensitivity[2]	$Sens_{TA}$	Over full range of I_P, T_A = 25°C	–	66	–	mV/A
	$Sens_{TOP}$	Over full range of I_P	64	–	68	mV/A
Noise	$V_{NOISE(PP)}$	Peak-to-peak, T_A= 25°C, 66 mV/A programmed Sensitivity, C_F=4.7 nF, C_{OUT} = open, 20 kHz bandwidth	–	20	–	mV
		Peak-to-peak, T_A = 25°C, 66 mV/A programmed Sensitivity, C_F = 47 nF, C_{OUT} = open, 2 kHz bandwidth	–	7	–	mV
		Peak-to-peak, T_A = 25°C, 66 mV/A programmed Sensitivity, C_F = 1 nF, C_{OUT} = open, 50 kHz bandwidth	–	35	–	mV
Electrical Offset Voltage	V_{OE}	I_P = 0 A	–30	–	30	mV
Total Output Error[3]	E_{TOT}	I_P = ±30 A, T_A = 25°C	–	±1.5	–	%

[1]Device may be operated at higher primary current levels, I_P, and ambient temperatures, T_{OP}, provided that the Maximum Junction Temperature, T_J(max), is not exceeded.
[2]At –40°C Sensitivity may shift as much 9% outside of the datasheet limits.
[3]Percentage of I_P, with I_P = 30 A. Output filtered.

Characteristic Performance

I_P = 5 A, Sens = 185 mV/A unless otherwise specified

Mean Supply Current versus Ambient Temperature

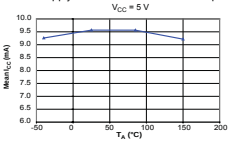

Supply Current versus Supply Voltage

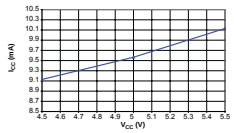

Magnetic Offset versus Ambient Temperature

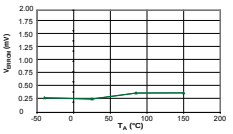

Nonlinearity versus Ambient Temperature

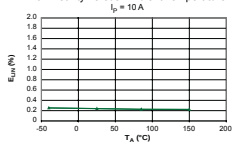

Mean Total Output Error versus Ambient Temperature

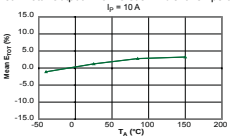

Output Voltage versus Sensed Current

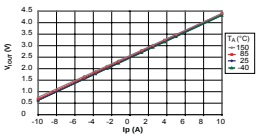

Sensitivity versus Sensed Current

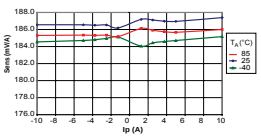

Characteristic Performance

I_P = 30 A, Sens = 66 mV/A unless otherwise specified

Mean Supply Current versus Ambient Temperature

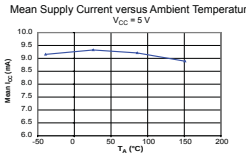

Supply Current versus Supply Voltage

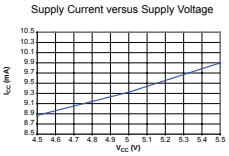

Magnetic Offset Current versus Ambient Temperature

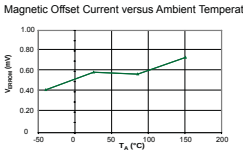

Nonlinearity versus Ambient Temperature

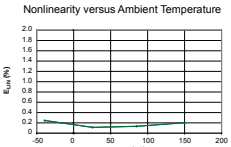

Mean Total Output Error versus Ambient Temperature

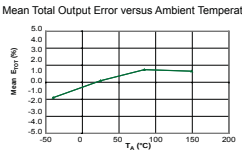

Output Voltage versus Sensed Current

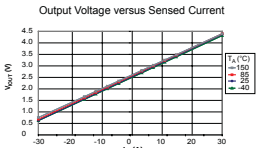

Sensitivity versus Sensed Current

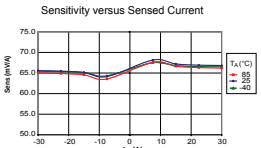

Definitions of Accuracy Characteristics

Sensitivity (Sens). The change in sensor output in response to a 1A change through the primary conductor. The sensitivity is the product of the magnetic circuit sensitivity (G/A) and the linear IC amplifier gain (mV/G). The linear IC amplifier gain is programmed at the factory to optimize the sensitivity (mV/A) for the full-scale current of the device.

Noise (V_{NOISE}). The product of the linear IC amplifier gain (mV/G) and the noise floor for the Allegro Hall effect linear IC (≈1 G). The noise floor is derived from the thermal and shot noise observed in Hall elements. Dividing the noise (mV) by the sensitivity (mV/A) provides the smallest current that the device is able to resolve.

Linearity (E_{LIN}). The degree to which the voltage output from the sensor varies in direct proportion to the primary current through its full-scale amplitude. Nonlinearity in the output can be attributed to the saturation of the flux concentrator approaching the full-scale current. The following equation is used to derive the linearity:

$$100\left\{1-\left[\frac{\Delta \text{ gain} \times \%\text{ sat}\,(V_{\text{IOUT\_full-scale amperes}} - V_{\text{IOUT(Q)}})}{2\,(V_{\text{IOUT\_half-scale amperes}} - V_{\text{IOUT(Q)}})}\right]\right\}$$

where $V_{\text{IOUT\_full-scale amperes}}$ = the output voltage (V) when the sensed current approximates full-scale ±I_P.

Symmetry (E_{SYM}). The degree to which the absolute voltage output from the sensor varies in proportion to either a positive or negative full-scale primary current. The following formula is used to derive symmetry:

$$100\left(\frac{V_{\text{IOUT\_+ full-scale amperes}} - V_{\text{IOUT(Q)}}}{V_{\text{IOUT(Q)}} - V_{\text{IOUT\_–full-scale amperes}}}\right)$$

Quiescent output voltage ($V_{IOUT(Q)}$). The output of the sensor when the primary current is zero. For a unipolar supply voltage, it nominally remains at V_{CC}/2. Thus, V_{CC} = 5 V translates into $V_{IOUT(Q)}$ = 2.5 V. Variation in $V_{IOUT(Q)}$ can be attributed to the resolution of the Allegro linear IC quiescent voltage trim and thermal drift.

Electrical offset voltage (V_{OE}). The deviation of the device output from its ideal quiescent value of V_{CC}/ 2 due to nonmagnetic causes. To convert this voltage to amperes, divide by the device sensitivity, Sens.

Accuracy (E_{TOT}). The accuracy represents the maximum deviation of the actual output from its ideal value. This is also known as the total ouput error. The accuracy is illustrated graphically in the output voltage versus current chart at right.

Accuracy is divided into four areas:

- **0 A at 25°C.** Accuracy of sensing zero current flow at 25°C, without the effects of temperature.
- **0 A over Δ temperature.** Accuracy of sensing zero current flow including temperature effects.
- **Full-scale current at 25°C.** Accuracy of sensing the full-scale current at 25°C, without the effects of temperature.
- **Full-scale current over Δ temperature.** Accuracy of sensing full-scale current flow including temperature effects.

Ratiometry. The ratiometric feature means that its 0 A output, $V_{IOUT(Q)}$, (nominally equal to V_{CC}/2) and sensitivity, Sens, are proportional to its supply voltage, V_{CC}. The following formula is used to derive the ratiometric change in 0 A output voltage, $\Delta V_{IOUT(Q)RAT}$ (%).

$$100\left(\frac{V_{\text{IOUT(Q)VCC}} / V_{\text{IOUT(Q)5V}}}{V_{\text{CC}} / 5\text{ V}}\right)$$

The ratiometric change in sensitivity, $\Delta Sens_{RAT}$ (%), is defined as:

$$100\left(\frac{Sens_{\text{VCC}} / Sens_{\text{5V}}}{V_{\text{CC}} / 5\text{ V}}\right)$$

Output Voltage versus Sensed Current
Accuracy at 0 A and at Full-Scale Current

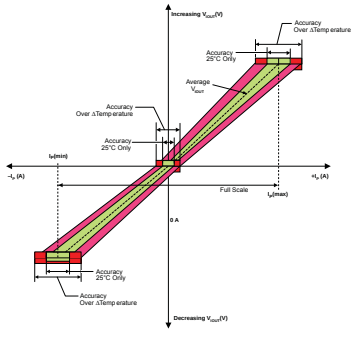

Definitions of Dynamic Response Characteristics

Propagation delay (t_{PROP}). The time required for the sensor output to reflect a change in the primary current signal. Propagation delay is attributed to inductive loading within the linear IC package, as well as in the inductive loop formed by the primary conductor geometry. Propagation delay can be considered as a fixed time offset and may be compensated.

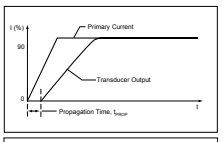

Response time ($t_{RESPONSE}$). The time interval between a) when the primary current signal reaches 90% of its final value, and b) when the sensor reaches 90% of its output corresponding to the applied current.

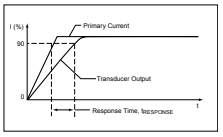

Rise time (t_r). The time interval between a) when the sensor reaches 10% of its full scale value, and b) when it reaches 90% of its full scale value. The rise time to a step response is used to derive the bandwidth of the current sensor, in which $f(-3\text{ dB}) = 0.35/t_r$. Both t_r and $t_{RESPONSE}$ are detrimentally affected by eddy current losses observed in the conductive IC ground plane.

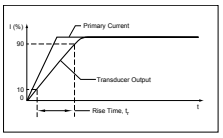

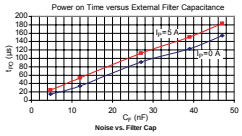

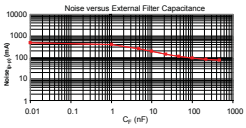

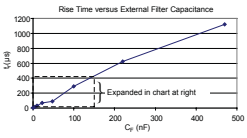

C_F (nF)	t_r (µs)
0	6.6
1	7.7
4.7	17.4
10	32.1
22	68.2
47	88.2
100	291.3
220	623.0
470	1120.0

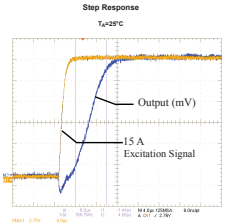

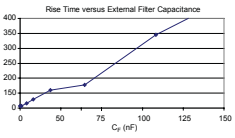

Chopper Stabilization Technique

Chopper Stabilization is an innovative circuit technique that is used to minimize the offset voltage of a Hall element and an associated on-chip amplifier. Allegro patented a Chopper Stabilization technique that nearly eliminates Hall IC output drift induced by temperature or package stress effects. This offset reduction technique is based on a signal modulation-demodulation process. Modulation is used to separate the undesired dc offset signal from the magnetically induced signal in the frequency domain. Then, using a low-pass filter, the modulated dc offset is suppressed while the magnetically induced signal passes through the filter. As a result of this chopper stabilization approach, the output voltage from the Hall IC is desensitized to the effects of temperature and mechanical stress. This technique produces devices that have an extremely stable Electrical Offset Voltage, are immune to thermal stress, and have precise recoverability after temperature cycling.

This technique is made possible through the use of a BiCMOS process that allows the use of low-offset and low-noise amplifiers in combination with high-density logic integration and sample and hold circuits.

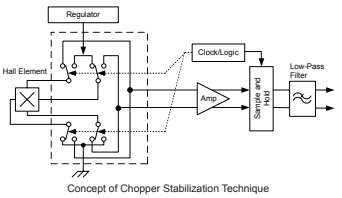

Concept of Chopper Stabilization Technique

Typical Applications

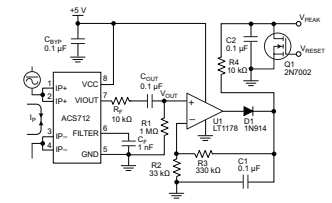

Application 2. Peak Detecting Circuit

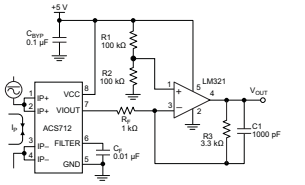

Application 3. This configuration increases gain to 610 mV/A (tested using the ACS712ELC-05A).

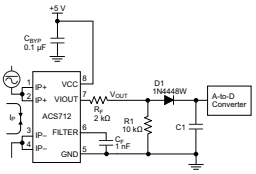

Application 4. Rectified Output. 3.3 V scaling and rectification application for A-to-D converters. Replaces current transformer solutions with simpler ACS circuit. C1 is a function of the load resistance and filtering desired. R1 can be omitted if the full range is desired.

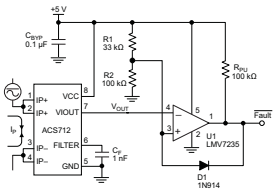

Application 5. 10 A Overcurrent Fault Latch. Fault threshold set by R1 and R2. This circuit latches an overcurrent fault and holds it until the 5 V rail is powered down.

Improving Sensing System Accuracy Using the FILTER Pin

In low-frequency sensing applications, it is often advantageous to add a simple RC filter to the output of the sensor. Such a low-pass filter improves the signal-to-noise ratio, and therefore the resolution, of the sensor output signal. However, the addition of an RC filter to the output of a sensor IC can result in undesirable sensor output attenuation — even for dc signals.

Signal attenuation, ΔV_{ATT}, is a result of the resistive divider effect between the resistance of the external filter, R_F (see Application 6), and the input impedance and resistance of the customer interface circuit, R_{INTFC}. The transfer function of this resistive divider is given by:

$$\Delta V_{ATT} = V_{IOUT}\left(\frac{R_{INTFC}}{R_F + R_{INTFC}}\right) .$$

Even if R_F and R_{INTFC} are designed to match, the two individual resistance values will most likely drift by different amounts over temperature. Therefore, signal attenuation will vary as a function of temperature. Note that, in many cases, the input impedance, R_{INTFC}, of a typical analog-to-digital converter (ADC) can be as low as 10 kΩ.

The ACS712 contains an internal resistor, a FILTER pin connection to the printed circuit board, and an internal buffer amplifier. With this circuit architecture, users can implement a simple RC filter via the addition of a capacitor, C_F (see Application 7) from the FILTER pin to ground. The buffer amplifier inside of the ACS712 (located after the internal resistor and FILTER pin connection) eliminates the attenuation caused by the resistive divider effect described in the equation for ΔV_{ATT}. Therefore, the ACS712 device is ideal for use in high-accuracy applications that cannot afford the signal attenuation associated with the use of an external RC low-pass filter.

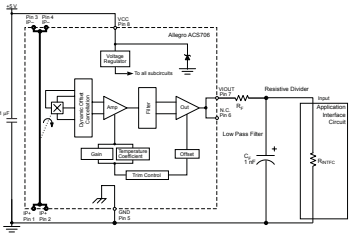

Application 6. When a low pass filter is constructed externally to a standard Hall effect device, a resistive divider may exist between the filter resistor, R_F, and the resistance of the customer interface circuit, R_{INTFC}. This resistive divider will cause excessive attenuation, as given by the transfer function for ΔV_{ATT}.

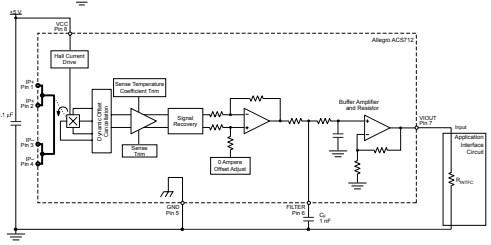

Application 7. Using the FILTER pin provided on the ACS712 eliminates the attenuation effects of the resistor divider between R_F and R_{INTFC}, shown in Application 6.

Package LC, 8-pin SOIC

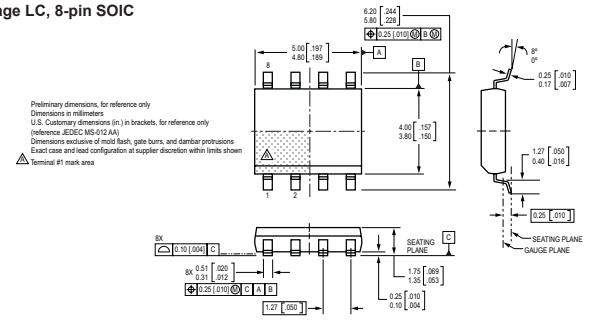

Package Branding

Two alternative patterns are used

ACS712T *RLCPPP YYWWA*	ACS	Allegro Current Sensor
	712	Device family number
	T	Indicator of 100% matte tin leadframe plating
	R	Operating ambient temperature range code
	LC	Package type designator
	PPP	Primary sensed current
	YY	Date code: Calendar year (last two digits)
	WW	Date code: Calendar week
	A	Date code: Shift code

ACS712T *RLCPPP L…L YYWW*	ACS	Allegro Current Sensor
	712	Device family number
	T	Indicator of 100% matte tin leadframe plating
	R	Operating ambient temperature range code
	LC	Package type designator
	PPP	Primary sensed current
	L…L	Lot code
	YY	Date code: Calendar year (last two digits)
	WW	Date code: Calendar week

For the latest version of this document, go to our website at:
www.allegromicro.com

D

Datasheet: Level Shifter

TEXAS INSTRUMENTS

Data sheet acquired from Harris Semiconductor
SCHS099B – Revised January 2003

CD40109B Types

CMOS Quad Low-to-High Voltage Level Shifter

High-Voltage Types (20-Volt Rating)

■ **CD40109B contains four low-to-high-voltage level-shifting circuits. Each circuit will shift a low-voltage digital-logic input signal (A, B, C, D) with logical 1 = V_{CC} and logical 0 = V_{SS} to a higher-voltage output signal (E, F, G, H) with logical 1 = V_{DD} and logical 0 = V_{SS}.**

The CD40109, unlike other low-to-high level-shifting circuits, does not require the presence of the high-voltage supply (V_{DD}) before the application of either the low-voltage supply (V_{CC}) or the input signals. There are no restrictions on the sequence of application of V_{DD}, V_{CC}, or the input signals. In addition, with one exception there are no restrictions on the relative magnitudes of the supply voltages or input signals within the device maximum ratings, provided that the input signal swings between V_{SS} and at least 0.7 V_{CC}; V_{CC} may exceed V_{DD}, and input signals may exceed V_{CC} and V_{DD}. When operated in the mode $V_{CC} > V_{DD}$, the CD40109 will operate as a high-to-low level-shifter.

The CD40109 also features individual three-state output capability. A low level on any of the separately enabled three-state output controls produces a high-impedance state in the corresponding output.

The CD40109B-Series types are supplied in 16-lead ceramic dual-in-line packages (F3A suffix), 16-lead dual-in-line plastic packages (E suffix), 16-lead small-outline packages (NSR suffix), and 16-lead thin shrink small-outline packages (PW and PWR suffixes).

Applications:

- **High-or-low level-shifting with three-state outputs for unidirectional or bidirectional bussing**
- **Isolation of logic subsystems using separate power supplies from supply sequencing, supply loss and supply regulation considerations**

Features:

- **Independence of power supply sequence considerations—V_{CC} can exceed V_{DD}, input signals can exceed both V_{CC} and V_{DD}**
- **Up and down level-shifting capability**
- **Three-state outputs with separate enable controls**
- **Standardized, symmetrical output characteristics**
- **100% tested for quiescent current at 20 V**
- **Maximum input current of 1 μA at 18 V over full package-temperature range; 100 nA at 18 V and 25°C**
- **Noise margin (full package-temperature range)**
  = 1 V at V_{CC} = 5 V, V_{DD} = 10 V
  = 2 V at V_{CC} = 10 V, V_{DD} = 15 V
- **5-V, 10-V, and 15-V parametric ratings**
- **Meets all requirements of JEDEC Tentative Standard No. 13B, "Standard Specifications for Description of 'B' Series CMOS Devices"**

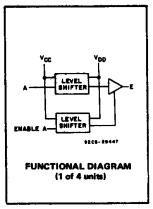

FUNCTIONAL DIAGRAM (1 of 4 units)

RECOMMENDED OPERATING CONDITIONS

For maximum reliability, nominal operating conditions should be selected so that operation is always within the following ranges:

CHARACTERISTIC	LIMITS		UNITS
	MIN.	MAX.	
Supply-Voltage Range (For T_A = Full Package-Temperature Range)	3	18	V

MAXIMUM RATINGS, *Absolute-Maximum Values:*

DC SUPPLY-VOLTAGE RANGE, (V_{DD})
Voltages referenced to V_{SS} Terminal) ..... -0.5V to +20V
OUTPUT VOLTAGE RANGE, ALL OUTPUTS ..... -0.5 V to V_{DD} +0.5 V
DC INPUT CURRENT, ANY ONE INPUT ..... ±10mA
POWER DISSIPATION PER PACKAGE (P_D):
For T_A = -55°C to +100°C 500mW
For T_A = +100°C to +125°C ..... Derate Linearity at 12mW/°C to 200mW
DEVICE DISSIPATION PER OUTPUT TRANSISTOR
FOR T_A = FULL PACKAGE-TEMPERATURE RANGE (All Package Types) 100mW
OPERATING-TEMPERATURE RANGE (T_A) ..... -55°C to +125°C
STORAGE TEMPERATURE RANGE (T_{stg}) ..... -65°C to +150°C
LEAD TEMPERATURE (DURING SOLDERING):
At distance 1/16 ± 1/32 inch (1.59 ± 0.79mm) from case for 10s max ..... +265°C

TRUTH TABLE

INPUTS		OUTPUTS
A, B, C, D	ENABLE A, B, C, D	E, F, G, H
0	1	0
1	1	1
X	0	Z

LOGIC 0 = LOW(V_{SS}) X = DON'T CARE Z = HIGH IMPEDANCE
LOGIC 1 = V_{CC} at INPUTS and V_{DD} at OUTPUTS

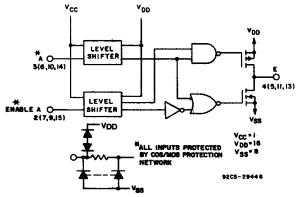

Fig. 1 – CD40109B logic diagram (1 of 4 units).

STATIC ELECTRICAL CHARACTERISTICS

CHARACTERISTIC	CONDITIONS			LIMITS AT INDICATED TEMPERATURES (°C)							UNITS
								+25			
	V_O (V)	V_{IN} (V)	V_{DD} (V)	-55	-40	+85	+125	Min.	Typ.	Max.	
Quiescent Device Current, I_{DD} Max.	–	0,5	5	1	1	30	30	–	0.02	1	μA
	–	0,10	10	2	2	60	60	–	0.02	2	
	–	0,15	15	4	4	120	120	–	0.02	4	
	–	0,20	20	20	20	600	600	–	0.04	20	
Output Low (Sink) Current I_{OL} Min.	0.4	0,5	5	0.64	0.61	0.42	0.36	0.51	1	–	mA
	0.5	0,10	10	1.6	1.5	1.1	0.9	1.3	2.6	–	
	1.5	0,15	15	4.2	4	2.8	2.4	3.4	6.8	–	
Output High (Source) Current, I_{OH} Min.	4.6	0,5	5	-0.64	-0.61	-0.42	-0.36	-0.51	-1	–	
	2.5	0,5	5	-2	-1.8	-1.3	-1.15	-1.6	-3.2	–	
	9.5	0,10	10	-1.6	-1.5	-1.1	-0.9	-1.3	-2.6	–	
	13.5	0,15	15	-4.2	-4	-2.8	-2.4	-3.4	-6.8	–	
Output Voltage: Low-Level, V_{OL} Max.	–	0,5	5	0.05				–	0	0.05	V
	–	0,10	10	0.05				–	0	0.05	
	–	0,15	15	0.05				–	0	0.05	
Output Voltage: High-Level, V_{OH} Min.	–	0,5	5	4.95				4.95	5	–	
	–	0,10	10	9.95				9.95	10	–	
	–	0,15	15	14.95				14.95	15	–	
Input Current I_{IN} Max.		0,18	18	±0.1	±0.1	±1	±1	–	$\pm 10^{-5}$	±0.1	μA
3-State Output Leakage Current I_{OUT} Max.		0,18	18	±0.4	±0.4	±12	±12	–	$\pm 10^{-4}$	±0.4	μA
	V_O (V)	V_{CC} (V)	V_{DD} (V)								
Input Low Voltage, V_{IL} Max.	1,9	5	10	1.5				–	–	1.5	V
	1.5, 13.5	10	15	3				–	–	3	
Input High Voltage, V_{IH} Min.	1,9	5	10	3.5				3.5	–	–	
	1.5,13.5	10	15	7				7	–	–	

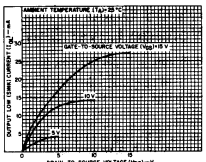

Fig.2 – Typical output low (sink) current characteristics.

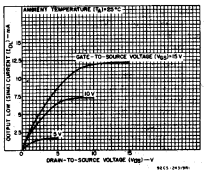

Fig.3 – Minimum output low (sink) current characteristics.

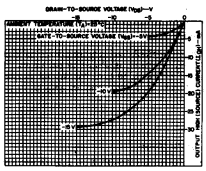

Fig.4 – Typical output high (source).

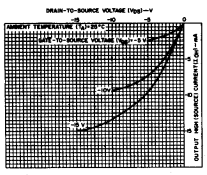

Fig.5 – Minimum output high (source) current characteristics.

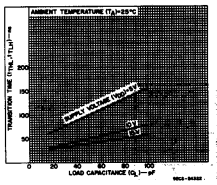

Fig.6 – Typical transition time as a function of load capacitance.

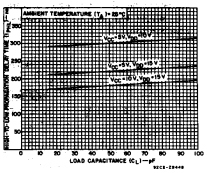

Fig.7 – Typical high-to-low propagation delay time as a function of load capacitance.

DYNAMIC ELECTRICAL CHARACTERISTICS at T_A = 25°C, Input t_r, t_f = 20 ns, C_L = 50 pF, R_L = 200 kΩ unless otherwise specified

CHARACTERISTIC	SHIFTING MODE	V_{CC} (V)	V_{DD} (V)	LIMITS Typ.	LIMITS Max.	UNITS
Propagation Delay – Data Input to Output: High-to-Low Level, t_{PHL}	L–H	5	10	300	600	ns
		10	15	220	440	
		15	15	180	360	
	H–L	10	5	250	500	
		15	5	250	500	
		15	10	120	240	
Low-to-High Level, t_{PLH}	L–H	5	10	130	260	ns
		5	15	120	240	
		10	15	70	140	
	H–L	10	5	230	460	
		15	5	230	460	
		15	10	80	160	
3-State Disable Delay: R_L = 1 kΩ Output High to High Impedance, t_{PHZ}	L–H	5	10	60	120	ns
		5	15	75	150	
		10	15	35	70	
	H–L	10	5	200	400	
		15	5	200	400	
		15	10	40	80	
Output Low to High Impedance, t_{PLZ}	L–H	5	10	370	740	ns
		5	15	300	600	
		10	15	250	500	
	H–L	10	5	250	500	
		15	5	250	500	
		15	10	130	260	
High Impedance to Output High, t_{PZH}	L–H	5	10	320	640	ns
		5	15	230	460	
		10	15	180	360	
	H–L	10	5	300	600	
		15	5	300	600	
		15	10	130	260	
High Impedance to Output Low, t_{PZL}	L–H	5	10	100	200	ns
		5	15	80	160	
		10	15	40	80	
	H–L	10	5	200	400	
		15	5	200	400	
		15	10	40	80	
Transition Time, t_{THL}, t_{TLH}	L–H	5	10	50	100	ns
		5	15	40	80	
		10	15	40	80	
	H–L	10	5	100	200	
		15	5	100	200	
		15	10	50	100	
Input Capacitance, C_I		Any Input		5	7.5	pF

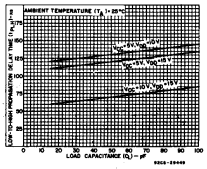

Fig.8 – Typical low-to-high propagation delay time as a function of load capacitance.

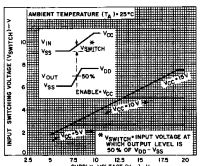

Fig.9 – Typical input switching as a function of high-level supply voltage.

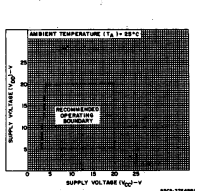

Fig.10 – High-level supply voltage vs. low-level supply voltage.

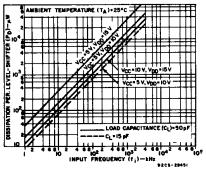

Fig.11 – Typical dynamic power dissipation as a function of input frequency.

TEST CIRCUITS

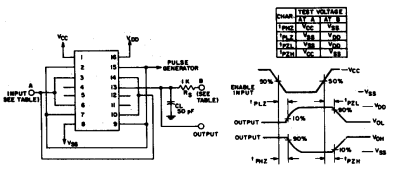

Fig. 12 – Output enable delay times test circuit and waveforms.

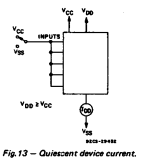

Fig.13 – Quiescent device current.

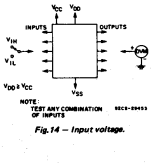

Fig. 14 – Input voltage.

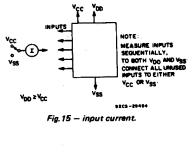

Fig. 15 – input current.

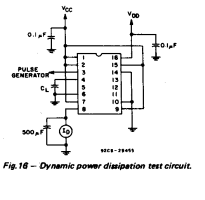

Fig. 16 – Dynamic power dissipation test circuit.

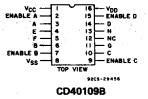

CD40109B TERMINAL ASSIGNMENT

Dimensions in parentheses are in millimeters and are derived from the basic inch dimensions as indicated. Grid graduations are in mils (10^{-3} inch).

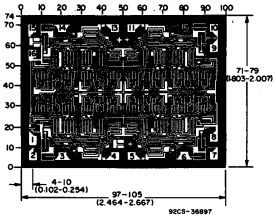

Dimensions and pad layout for CD40109BH.

PACKAGING INFORMATION

Orderable Device	Status [1]	Package Type	Package Drawing	Pins	Package Qty	Eco Plan [2]	Lead/ Ball Finish	MSL Peak Temp [3]	Samples (Requires Login)
CD40109BE	ACTIVE	PDIP	N	16	25	Pb-Free (RoHS)	CU NIPDAU	N / A for Pkg Type	
CD40109BEE4	ACTIVE	PDIP	N	16	25	Pb-Free (RoHS)	CU NIPDAU	N / A for Pkg Type	
CD40109BF	ACTIVE	CDIP	J	16	1	TBD	A42	N / A for Pkg Type	
CD40109BF3A	ACTIVE	CDIP	J	16	1	TBD	A42	N / A for Pkg Type	
CD40109BK3	OBSOLETE	CFP	WR	16		TBD	Call TI	Call TI	
CD40109BNSR	ACTIVE	SO	NS	16	2000	Green (RoHS & no Sb/Br)	CU NIPDAU	Level-1-260C-UNLIM	
CD40109BNSRE4	ACTIVE	SO	NS	16	2000	Green (RoHS & no Sb/Br)	CU NIPDAU	Level-1-260C-UNLIM	
CD40109BNSRG4	ACTIVE	SO	NS	16	2000	Green (RoHS & no Sb/Br)	CU NIPDAU	Level-1-260C-UNLIM	
CD40109BPW	ACTIVE	TSSOP	PW	16	90	Green (RoHS & no Sb/Br)	CU NIPDAU	Level-1-260C-UNLIM	
CD40109BPWE4	ACTIVE	TSSOP	PW	16	90	Green (RoHS & no Sb/Br)	CU NIPDAU	Level-1-260C-UNLIM	
CD40109BPWG4	ACTIVE	TSSOP	PW	16	90	Green (RoHS & no Sb/Br)	CU NIPDAU	Level-1-260C-UNLIM	
CD40109BPWR	ACTIVE	TSSOP	PW	16	2000	Green (RoHS & no Sb/Br)	CU NIPDAU	Level-1-260C-UNLIM	
CD40109BPWRE4	ACTIVE	TSSOP	PW	16	2000	Green (RoHS & no Sb/Br)	CU NIPDAU	Level-1-260C-UNLIM	
CD40109BPWRG4	ACTIVE	TSSOP	PW	16	2000	Green (RoHS & no Sb/Br)	CU NIPDAU	Level-1-260C-UNLIM	

[1] The marketing status values are defined as follows:
ACTIVE: Product device recommended for new designs.
LIFEBUY: TI has announced that the device will be discontinued, and a lifetime-buy period is in effect.
NRND: Not recommended for new designs. Device is in production to support existing customers, but TI does not recommend using this part in a new design.
PREVIEW: Device has been announced but is not in production. Samples may or may not be available.
OBSOLETE: TI has discontinued the production of the device.

[2] Eco Plan - The planned eco-friendly classification: Pb-Free (RoHS), Pb-Free (RoHS Exempt), or Green (RoHS & no Sb/Br) - please check http://www.ti.com/productcontent for the latest availability information and additional product content details.
TBD: The Pb-Free/Green conversion plan has not been defined.

TEXAS INSTRUMENTS
www.ti.com
PACKAGE OPTION ADDENDUM
30-Jan-2012

Pb-Free (RoHS): TI's terms "Lead-Free" or "Pb-Free" mean semiconductor products that are compatible with the current RoHS requirements for all 6 substances, including the requirement that lead not exceed 0.1% by weight in homogeneous materials. Where designed to be soldered at high temperatures, TI Pb-Free products are suitable for use in specified lead-free processes.
Pb-Free (RoHS Exempt): This component has a RoHS exemption for either 1) lead-based flip-chip solder bumps used between the die and package, or 2) lead-based die adhesive used between the die and leadframe. The component is otherwise considered Pb-Free (RoHS compatible) as defined above.
Green (RoHS & no Sb/Br): TI defines "Green" to mean Pb-Free (RoHS compatible), and free of Bromine (Br) and Antimony (Sb) based flame retardants (Br or Sb do not exceed 0.1% by weight in homogeneous material)

[3] MSL, Peak Temp. -- The Moisture Sensitivity Level rating according to the JEDEC industry standard classifications, and peak solder temperature.

Important Information and Disclaimer: The information provided on this page represents TI's knowledge and belief as of the date that it is provided. TI bases its knowledge and belief on information provided by third parties, and makes no representation or warranty as to the accuracy of such information. Efforts are underway to better integrate information from third parties. TI has taken and continues to take reasonable steps to provide representative and accurate information but may not have conducted destructive testing or chemical analysis on incoming materials and chemicals. TI and TI suppliers consider certain information to be proprietary, and thus CAS numbers and other limited information may not be available for release.

In no event shall TI's liability arising out of such information exceed the total purchase price of the TI part(s) at issue in this document sold by TI to Customer on an annual basis.

OTHER QUALIFIED VERSIONS OF CD40109B, CD40109B-MIL :

- Catalog: CD40109B
- Automotive: CD40109B-Q1, CD40109B-Q1
- Military: CD40109B-MIL

NOTE: Qualified Version Definitions:

- Catalog - TI's standard catalog product
- Automotive - Q100 devices qualified for high-reliability automotive applications targeting zero defects
- Military - QML certified for Military and Defense Applications

TAPE AND REEL INFORMATION

REEL DIMENSIONS

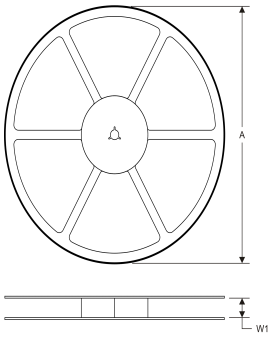

TAPE DIMENSIONS

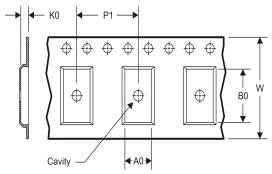

A0	Dimension designed to accommodate the component width
B0	Dimension designed to accommodate the component length
K0	Dimension designed to accommodate the component thickness
W	Overall width of the carrier tape
P1	Pitch between successive cavity centers

TAPE AND REEL INFORMATION

*All dimensions are nominal

Device	Package Type	Package Drawing	Pins	SPQ	Reel Diameter (mm)	Reel Width W1 (mm)	A0 (mm)	B0 (mm)	K0 (mm)	P1 (mm)	W (mm)	Pin1 Quadrant
CD40109BNSR	SO	NS	16	2000	330.0	16.4	8.2	10.5	2.5	12.0	16.0	Q1
CD40109BPWR	TSSOP	PW	16	2000	330.0	12.4	6.9	5.6	1.6	8.0	12.0	Q1

TEXAS INSTRUMENTS
www.ti.com
PACKAGE MATERIALS INFORMATION
28-Jan-2012

TAPE AND REEL BOX DIMENSIONS

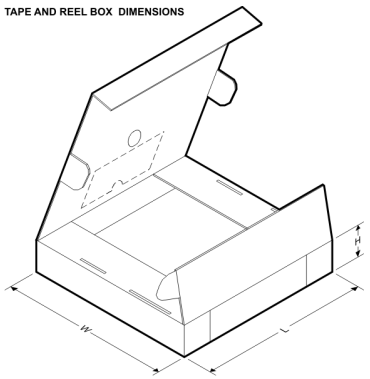

*All dimensions are nominal

Device	Package Type	Package Drawing	Pins	SPQ	Length (mm)	Width (mm)	Height (mm)
CD40109BNSR	SO	NS	16	2000	346.0	346.0	33.0
CD40109BPWR	TSSOP	PW	16	2000	346.0	346.0	29.0

J (R–GDIP–T**) CERAMIC DUAL IN–LINE PACKAGE

14 LEADS SHOWN

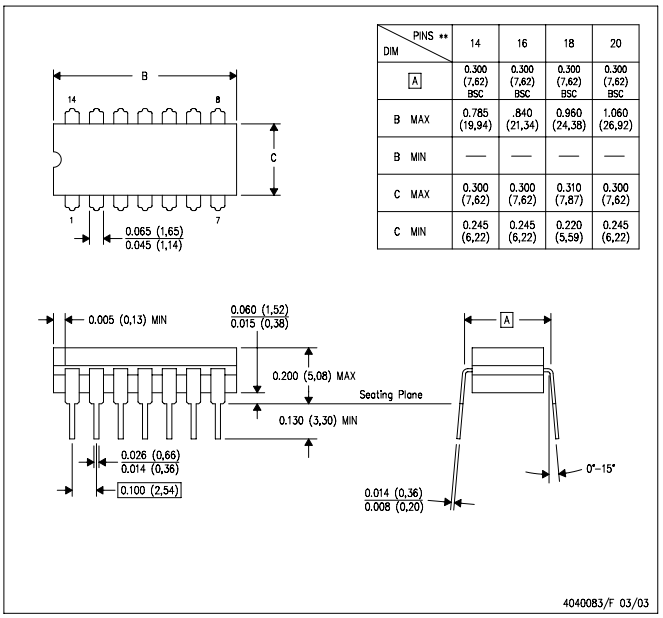

DIM \ PINS **	14	16	18	20
A	0.300 (7,62) BSC	0.300 (7,62) BSC	0.300 (7,62) BSC	0.300 (7,62) BSC
B MAX	0.785 (19,94)	.840 (21,34)	0.960 (24,38)	1.060 (26,92)
B MIN	—	—	—	—
C MAX	0.300 (7,62)	0.300 (7,62)	0.310 (7,87)	0.300 (7,62)
C MIN	0.245 (6,22)	0.245 (6,22)	0.220 (5,59)	0.245 (6,22)

4040083/F 03/03

NOTES:
A. All linear dimensions are in inches (millimeters).
B. This drawing is subject to change without notice.
C. This package is hermetically sealed with a ceramic lid using glass frit.
D. Index point is provided on cap for terminal identification only on press ceramic glass frit seal only.
E. Falls within MIL STD 1835 GDIP1–T14, GDIP1–T16, GDIP1–T18 and GDIP1–T20.

N (R–PDIP–T**) PLASTIC DUAL–IN–LINE PACKAGE

16 PINS SHOWN

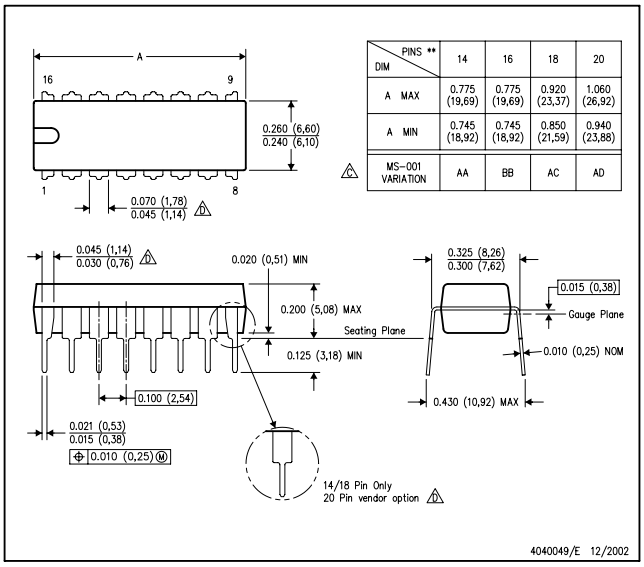

DIM \ PINS **	14	16	18	20
A MAX	0.775 (19,69)	0.775 (19,69)	0.920 (23,37)	1.060 (26,92)
A MIN	0.745 (18,92)	0.745 (18,92)	0.850 (21,59)	0.940 (23,88)
MS–001 VARIATION	AA	BB	AC	AD

4040049/E 12/2002

NOTES:
A. All linear dimensions are in inches (millimeters).
B. This drawing is subject to change without notice.
Falls within JEDEC MS–001, except 18 and 20 pin minimum body length (Dim A).
The 20 pin end lead shoulder width is a vendor option, either half or full width.

PW (R–PDSO–G16) PLASTIC SMALL OUTLINE

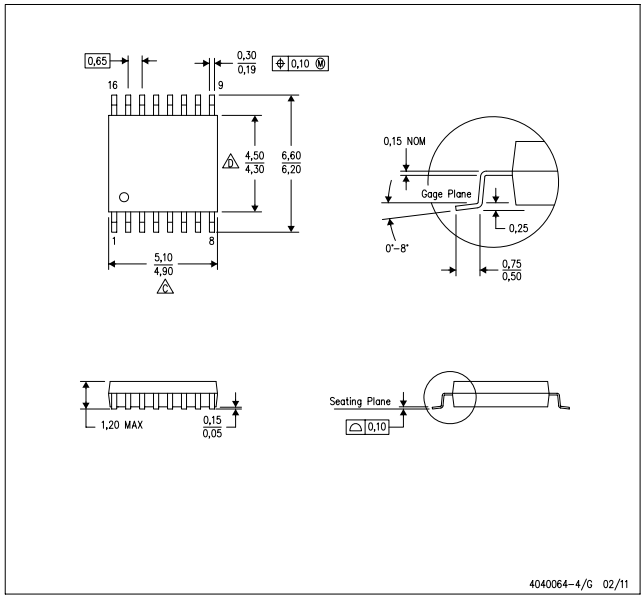

4040064–4/G 02/11

NOTES:
A. All linear dimensions are in millimeters. Dimensioning and tolerancing per ASME Y14.5M–1994.
B. This drawing is subject to change without notice.
Body length does not include mold flash, protrusions, or gate burrs. Mold flash, protrusions, or gate burrs shall not exceed 0,15 each side.
Body width does not include interlead flash. Interlead flash shall not exceed 0,25 each side.
E. Falls within JEDEC MO–153

PW (R–PDSO–G16) PLASTIC SMALL OUTLINE

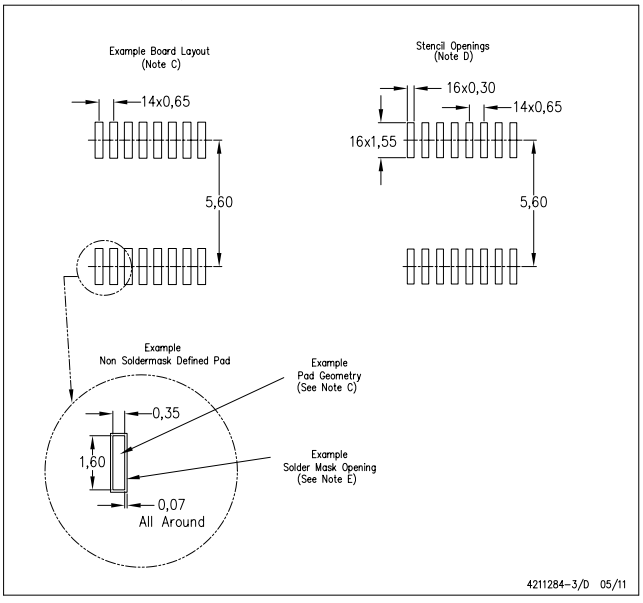

4211284–3/D 05/11

NOTES:
A. All linear dimensions are in millimeters.
B. This drawing is subject to change without notice.
C. Publication IPC–7351 is recommended for alternate designs.
D. Laser cutting apertures with trapezoidal walls and also rounding corners will offer better paste release. Customers should contact their board assembly site for stencil design recommendations. Refer to IPC–7525 for other stencil recommendations.
E. Customers should contact their board fabrication site for solder mask tolerances between and around signal pads.

MECHANICAL DATA

NS (R-PDSO-G)** **PLASTIC SMALL-OUTLINE PACKAGE**

14-PINS SHOWN

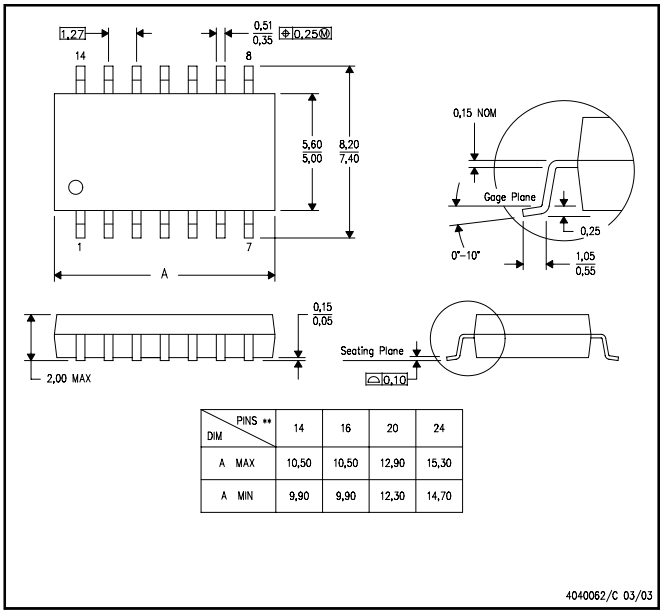

DIM \ PINS **	14	16	20	24
A MAX	10,50	10,50	12,90	15,30
A MIN	9,90	9,90	12,30	14,70

NOTES:
A. All linear dimensions are in millimeters.
B. This drawing is subject to change without notice.
C. Body dimensions do not include mold flash or protrusion, not to exceed 0,15.

TEXAS INSTRUMENTS
www.ti.com

IMPORTANT NOTICE

E

Datasheet: Motor Controller

VMA03

MANUAL HVMA03'1

Motor & Power shield Arduino®

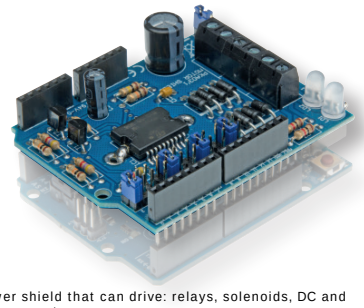

Power shield that can drive: relays, solenoids, DC and stepper motors

Features

- For use with Arduino Due™, Arduino Uno™, Arduino Mega™
- Based on L298P dual full bridge driver IC
- Outputs: up to 2 DC motors or 1 bipolar stepper motor
- Power supply: external power or power from Arduino board

Specifications

- Power supply: 7..46VDC
- Max current: 2A
- Dimensions: 68 x 53mm / 2.67 x 2.08"

Made for ARDUINO

Connection diagram

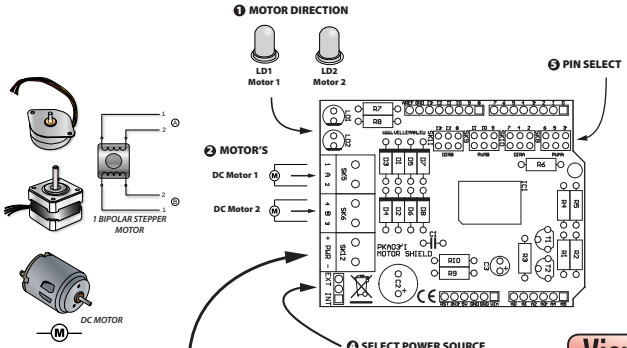

DOWNLOAD SAMPLE CODE FROM KA03 PAGE ON WWW.VELLEMAN.BE

View Forum

Participate our Velleman Projects Forum

Schematic diagram

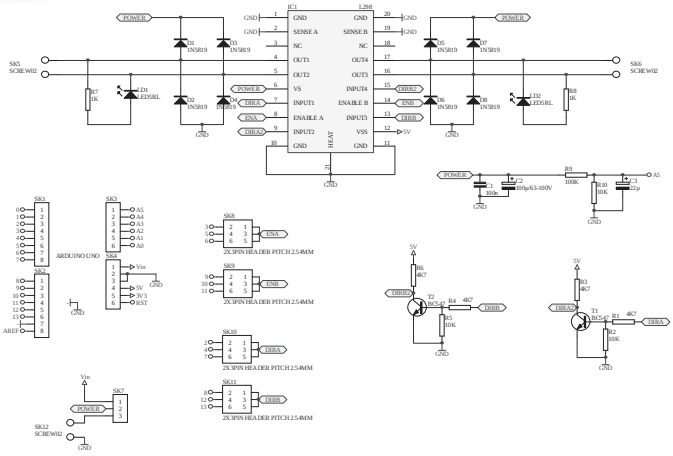

The new Velleman Projects catalogue is now available. Download your copy here: www.vellemanprojects.eu